

# AEC RESEARCH AND DEVELOPMENT REPORT

MARTIN MARIETTA ENERGY SYSTEMS LIBRARIES



3 4456 0251024 5

**CENTRAL RESEARCH LIBRARY  
DOCUMENT COLLECTION**

**LIBRARY LOAN COPY**

**DO NOT TRANSFER TO ANOTHER PERSON**

If you wish someone else to see this document,  
send in name with document and the library will  
arrange a loan.

AIRCRAFT NUCLEAR PROPULSION PROJECT

QUARTERLY PROGRESS REPORT

FOR PERIOD ENDING SEPTEMBER 10, 1956

**DECLASSIFIED**

CLASSIFICATION CHANGED TO:

BY AUTHORITY OF: *AEC 1-25-66*

BY: *C. Kachourista 2-14-67*



**OAK RIDGE NATIONAL LABORATORY**

OPERATED BY

**UNION CARBIDE NUCLEAR COMPANY**

A Division of Union Carbide and Carbon Corporation



POST OFFICE BOX X · OAK RIDGE, TENNESSEE



LEGAL NOTICE

This report was prepared as an account of Government sponsored work. Neither the United States, nor the Commission, nor any person acting on behalf of the Commission:

- A. Makes any warranty or representation, express or implied, with respect to the accuracy, completeness, or usefulness of the information contained in this report, or that the use of any information, apparatus, method, or process disclosed in this report may not infringe privately owned rights; or
- B. Assumes any liabilities with respect to the use of, or for damages resulting from the use of any information, apparatus, method, or process disclosed in this report.

As used in the above, "person acting on behalf of the Commission" includes any employee or contractor of the Commission to the extent that such employee or contractor prepares, handles or distributes, or provides access to, any information pursuant to his employment or contract with the Commission.

[REDACTED]

ORNL-2157, Part 6  
C-85 - Reactors - Aircraft Nuclear Propulsion Systems

This document consists of 52 pages.  
Copy 131 of 219 copies. Series A.

Contract No. W-7405-eng-26

AIRCRAFT NUCLEAR PROPULSION PROJECT

QUARTERLY PROGRESS REPORT

For Period Ending September 10, 1956

W. H. Jordan, Director  
S. J. Cromer, Co-Director  
A. J. Miller, Assistant Director

DATE ISSUED

MAR 1 1957

OAK RIDGE NATIONAL LABORATORY  
Operated by  
UNION CARBIDE NUCLEAR COMPANY  
A Division of Union Carbide and Carbon Corporation  
Post Office Box X  
Oak Ridge, Tennessee

[REDACTED]

[REDACTED]

[REDACTED]

MARTIN MARIETTA ENERGY SYSTEMS LIBRARIES



3 4456 0251024 5

[REDACTED]

ORNL-2157, Part 6  
C-85 - Reactors-Aircraft Nuclear Propulsion Systems

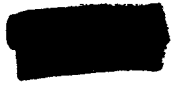
INTERNAL DISTRIBUTION

1. R. G. Affel
2. C. J. Barton
3. M. Bender
4. D. S. Billington
5. F. F. Blankenship
6. E. P. Blizard
7. C. J. Borkowski
8. W. F. Boudreau
9. G. E. Boyd
10. M. A. Bredig
11. E. J. Breeding
12. W. E. Browning
13. F. R. Bruce
14. A. D. Callihan
15. D. W. Cardwell
16. C. E. Center (K-25)
17. R. A. Charpie
18. R. L. Clarke
19. C. E. Clifford
20. J. H. Coobs
21. W. B. Cottrell
22. D. D. Cowen
23. S. Cromer
24. R. S. Crouse
25. F. L. Culler
26. D. R. Cuneo
27. J. H. DeVan
28. L. M. Doney
29. D. A. Douglas
30. E. R. Dytko
31. W. K. Eister
32. L. B. Emler (K-25)
33. D. E. Ferguson
34. A. P. Fraas
35. J. H. Frye
36. W. T. Furgerson
37. R. J. Gray
38. W. R. Grimes
39. A. G. Grindell
40. E. Guth
41. C. S. Harrill
42. E. E. Hoffman
43. H. W. Hoffman
44. A. Hollaender
45. A. S. Householder
46. J. T. Howe
47. W. H. Jordan
48. G. W. Keilholtz
49. C. P. Keim
50. F. L. Keller
51. M. T. Kelley
52. F. Kertesz
53. J. J. Keyes
54. E. M. King
- 55-56. J. A. Lane
57. R. B. Lindauer
58. R. S. Livingston
59. R. N. Lyon
60. H. G. MacPherson
61. R. E. MacPherson
62. F. C. Maienschein
63. W. D. Manly
64. E. R. Mann
65. L. A. Mann
66. W. B. McDonald
67. J. R. McNally
68. F. R. McQuilkin
69. R. V. Meghreblian
70. R. P. Milford
71. A. J. Miller
72. R. E. Moore
73. J. C. Morgan
74. K. Z. Morgan
75. E. J. Murphy
76. J. P. Murray (Y-12)
77. M. L. Nelson
78. G. J. Nettle
79. R. B. Oliver
80. L. G. Overholser
81. P. Patriarca
82. R. W. Peelle
83. S. K. Penny
84. A. M. Perry
85. J. C. Pigg
86. P. M. Reyling
87. A. E. Richt
88. M. T. Robinson
89. H. W. Savage
90. A. W. Savolainen
91. R. D. Schultheiss
92. D. Scott
93. E. D. Shipley

- 
- 94. A. Simon
  - 95. O. Sisman
  - 96. J. Sites
  - 97. M. J. Skinner
  - 98. A. H. Snell
  - 99. C. D. Susano
  - 100. J. A. Swartout
  - 101. E. H. Taylor
  - 102. R. E. Thoma
  - 103. D. B. Trauger
  - 104. D. K. Trubey
  - 105. G. M. Watson
  - 106. A. M. Weinberg
  - 107. J. C. White
  - 108. G. D. Whitman
  - 109. E. P. Wigner (consultant)
  - 110. G. C. Williams
  - 111. J. C. Wilson
  - 112. C. E. Winters
  - 113-122. ORNL – Y-12 Technical Library  
Document Reference Section
  - 123-129. Laboratory Records Department
  - 130. Laboratory Records, ORNL R.C.
  - 131-133. Central Research Library

#### EXTERNAL DISTRIBUTION

- 134. AF Plant Representative, Baltimore
- 135. AF Plant Representative, Burbank
- 136. AF Plant Representative, Marietta
- 137-139. AF Plant Representative, Santa Monica
- 140-141. AF Plant Representative, Seattle
- 142. AF Plant Representative, Wood-Ridge
- 143. Air Research and Development Command (RDGN)
- 144. Air Technical Intelligence Center
- 145. Air University Library
- 146. Allison Division
- 147-149. ANP Project Office, Fort Worth
- 150. Argonne National Laboratory
- 151. Armed Forces Special Weapons Project, Sandia
- 152. Armed Forces Special Weapons Project, Washington
- 153. Assistant Secretary of the Air Force, R&D
- 154-159. Atomic Energy Commission, Washington
- 160. Bureau of Aeronautics
- 161. Bureau of Aeronautics General Representative
- 162. Chicago Operations Office
- 163. Chicago Patent Group
- 164. Chief of Naval Research
- 165. Convair-General Dynamics Corporation
- 166-169. General Electric Company (ANPD)
- 170. Hartford Area Office
- 171. Headquarters, Air Force Special Weapons Center
- 172. Idaho Operations Office
- 173. Lockland Area Office
- 174. Los Alamos Scientific Laboratory
- 175. National Advisory Committee for Aeronautics, Cleveland
- 176. National Advisory Committee for Aeronautics, Washington
- 177. Naval Air Development and Material Center
- 178. Naval Research Laboratory
- 179. North American Aviation, Inc. (Aerophysics Division)
- 180. Nuclear Development Corporation of America
- 181. Office of Chief of Naval Operations (OP-361)
- 182. Patent Branch, Washington



- 183-186. Pratt & Whitney Aircraft Division (Fox Project)
- 187. Sandia Corporation
- 188. School of Aviation Medicine
- 189. USAF Project RAND
- 190. University of California Radiation Laboratory, Livermore
- 191-208. Wright Air Development Center (WCOSI-3)
- 209-218. Technical Information Service Extension, Oak Ridge
- 219. Division of Research and Development, AEC, ORO





### FOREWORD

This portion, Part 6. Advanced Power Plant Design and Aircraft Shielding, of the Aircraft Nuclear Propulsion Project Quarterly Progress Report falls in AEC category C-85, Reactors - Aircraft Nuclear Propulsion Systems, and is therefore being issued separately in order not to further limit distribution of the material that falls in AEC category C-84, Reactors - Special Features of Aircraft Reactors, which has been issued as ORNL-2157, Parts 1-5.





-

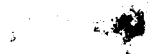
•

•

•

•

•





**CONTENTS**

FOREWORD..... v

SUMMARY ..... 1

PART 6. ADVANCED POWER PLANT DESIGN AND AIRCRAFT SHIELDING

6.1. ADVANCED POWER PLANT DESIGN..... 5

6.2. AIRCRAFT SHIELD DESIGN ..... 6

Calculation of the Gamma-Ray Dose Rates in Air and in a Crew Compartment  
Resulting from TSF Reactor Radiation..... 6

Dose Rates in Air from Direct Gamma Rays..... 7

Dose Rates in the Crew Compartment from Direct Gamma Rays ..... 11

Dose Rates in the Crew Compartment from Direct Gamma Rays Scattered in  
the Crew-Compartment Side Shielding..... 13

Dose Rates in the Crew Compartment from Air-Scattered Gamma Rays ..... 18

Dose Rates in Air and in the Crew Compartment from Air-Capture Gamma Rays ..... 23

Comparison of the Total Calculated Dose Rate with the Measured Dose Rate..... 32

Optimization of a Divided Neutron and Gamma-Ray Shield Over a Mission Profile ..... 36

Optimization of the Neutron Shield ..... 37

Optimization of the Gamma-Ray Shield ..... 38





# ANP PROJECT QUARTERLY PROGRESS REPORT

## SUMMARY

### PART 6. ADVANCED POWER PLANT DESIGN AND AIRCRAFT SHIELDING

#### 6.1. Advanced Power Plant Design

A review of ORSORT student summer project information on a rubidium-vapor-cycle compressor-jet engine coupled to a hydride-moderated circulating-fuel reactor is being made. Performance data were defined by the students in terms of specific impulse and specific heat consumption. These data are being supplemented by plots of cycle performance data and estimates of the weight of propulsion machinery.

#### 6.2. Aircraft Shield Design

**Calculation of the Gamma-Ray Dose Rates in Air and in a Crew Compartment Resulting from TSF Reactor Radiation.** – A calculation of the gamma-ray dose rate in an aircraft crew-compartment mockup has been made for comparison with the dose rate that was previously measured in the mockup at the Tower Shielding Facility (TSF). The same geometry as that used in the experiment was assumed for the calculation; that is, the radiation source was the TSF reactor, which was contained in a 12-ft-dia water tank, and the crew compartment was the mockup of the GE-ANP crew shield. The calculated total gamma-ray dose rate was necessarily the sum of the estimates of the dose rates from various sources. The sources considered were (1) the direct-beam gamma rays that penetrate the rear lead plug of the crew compartment, (2) the direct-beam gamma rays that penetrate the rear of the crew compartment outside the area of the lead plug and then scatter in the side-wall water shielding into the crew compartment, (3) the air-scattered gamma rays that penetrate the crew-compartment side shielding, and (4) the capture gamma rays produced in the air that penetrate the crew-compartment side shielding. The dose rate from capture gamma rays produced in the crew-compartment side shielding was not calculated, since there were no experimental values available for the thermal-neutron flux in the side shielding.

Three crew-compartment geometries were considered: case I, for which the crew side shielding consisted of water only; case II, for which the crew side shielding consisted of water plus a lead liner of staggered thickness; and case III, for which the crew side shielding consisted of water plus the lead liner of staggered thickness plus a lead liner of constant thickness. (There were no experimental results with which case II could be compared.) The rear lead plug was in position for all cases. Two reactor tank geometries were used, one for which  $\theta = 0$  deg and another for which  $\theta = 180$  deg. (The angle  $\theta$  gives the reactor orientation with respect to the reactor tank-crew compartment axis.)

In order to carry out this calculation, it was first necessary to determine the variation of the direct-beam gamma-ray dose rate in air as a function of angle around the reactor tank for various values of  $\rho$  ( $\rho$  = reactor water shield thickness). As would be expected, the plots of the calculated dose rates in air from the direct beam fit the experimental curves (in air) very well in the

region  $0 \leq \theta \leq 60$  deg. At larger angles the calculated curves are lower than the measured curves. This result is in agreement with the fact that the fraction of the measured dose rate which is contributed by the air-scattered gamma rays becomes important at the larger angles. The contribution of the direct beam to the dose rate inside the crew compartment was calculated to be 8 to 11% of the total measured dose rate for case I and  $\theta = 0$  deg. The contribution was 55 to 75% for case III. In general, except for small values of  $\rho$  at  $\theta = 180$  deg, the calculated dose rates resulting from the direct-beam radiation scattered in the crew-compartment side shield represented 20 to 40% of the total measured dose rates for cases I and III.

The dose rates resulting from air-scattered gamma rays were calculated for cases I and III and for a point in space. The purpose of the latter calculation was to determine the applicability of the single-scattering theory for predicting dose rates in air when used with the existing  $f(\psi)$  curves and known source angular strengths and source energy spectra. The general conclusion is that the single-scattering theory cannot be used to calculate accurately the air-scattered dose rates in geometries where the angular source strength is highly peaked away from the detector (for example, for  $\theta = 180$  deg). For  $\theta = 0$  deg the ratio of the contribution of the air-scattered dose rate to the total measured dose rate inside the crew compartment was 0.1 for case I and 0.06 for case III.

For  $\theta = 0$  deg the contribution of the air-capture gamma rays to the total dose rate in the crew compartment was significant for small values of  $\rho$ . For  $\theta = 180$  deg and small values of  $\rho$  the dose rate in the crew compartment resulted almost entirely from air-capture gamma rays. Plots of the contributions from the various sources are compared with the total calculated and total measured dose rates for the several cases.

**Optimization of a Divided Neutron and Gamma-Ray Shield Over a Mission Profile.** — The thicknesses and weights of a divided neutron and gamma-ray shield have been calculated for a specified total dose in a crew compartment rather than for a dose-rate restriction. The reactor was considered to be a Pratt & Whitney NJ-2A reactor, and the crew compartment was a 172-cm-dia by 500-cm cylinder. The total mission dose was specified as 26.67 rem in the crew compartment with a 3/1 ratio of the gamma-ray dose to the neutron dose. The mission profile included variations in altitude, reactor power, and fuel tank conditions. The results gave a total neutron shield of 9 tons, including 4.2 tons of alkylbenzene at the reactor and 4.7 tons of plastic at the crew compartment. The gamma-ray shield consisted of 6.5 tons of lead, including 2.2 tons at the reactor and 4.3 tons at the crew compartment.

Part 6

**ADVANCED POWER PLANT DESIGN**

S. J. Cromer

**AIRCRAFT SHIELDING**

E. P. Blizard



## 6.1. ADVANCED POWER PLANT DESIGN

A. P. Fraas

The ORSORT student summer project work on a hydride-moderated circulating-fuel reactor coupled to a rubidium-vapor-cycle compressor-jet engine went sufficiently far to define rather well the performance of the cycle in terms of specific impulse and specific heat consumption. A rough preliminary approximation of the reactor design was prepared. While the ORSORT group had to terminate their work, a small effort is continuing in order to complete the design study. The cycle performance data are being plotted in finished form, estimates of the weights of the various components of the propulsion machinery are being prepared, and, most important of all, the physics group is carrying out a much more thorough study of the hydride-moderated reactor core.

## 6.2. AIRCRAFT SHIELD DESIGN

C. E. Clifford

F. L. Keller

### CALCULATION OF THE GAMMA-RAY DOSE RATES IN AIR AND IN A CREW COMPARTMENT RESULTING FROM TSF REACTOR RADIATION

All the methods of shield design which are currently being employed for design of the nuclear-powered airplane shielding involve rather lengthy and intricate calculations of the gamma-ray dose rate expected in the crew compartment from radiation which leaves the reactor shield. All these methods involve calculations of the source strength of the reactor, the probabilities of the radiation being scattered in air, the number of gamma rays produced from air captures of thermal neutrons, the probabilities of radiation penetrating the crew compartment, etc. Most of these calculations have been carried out for very complex geometries, and, in the few cases for which it has been possible to make a direct comparison between prediction and measurement, very large discrepancies have often occurred. Because of the complexity of most of the configurations for which comparisons have been made, it has been difficult to determine the real reasons for the discrepancies. Hence it appeared that a detailed comparison should be made between the predicted and measured crew-compartment dose rates for some of the simple geometries which could be studied at the Tower Shielding Facility (TSF). These geometries are flexible enough to encompass extreme variations in the contributions to the dose rate from the several sources, such as air-scattered gamma rays, air-capture gamma rays, direct-beam gamma rays, etc.

The following contributions to the measured gamma-ray dose rate in the crew compartment were considered in the calculations: (1) the contributions from direct-beam gamma rays which strike the rear of the crew compartment and enter through the rear lead plug of the crew compartment, (2) the contribution from direct-beam gamma rays which strike the rear of the crew compartment in the region outside the area of the lead plug and then scatter from the water along the side of the crew compartment to the detector, (3) the contribution from gamma rays which scatter in the air and then enter the crew compartment through the side walls, and (4) the contribution from gamma rays produced by the capture of thermal neutrons by the nitrogen in the air.

A comparison was also made of calculated and measured dose rates in air outside the crew compartment for various positions of the reactor in the reactor tank. This comparison was useful in that it indicated the inadequacy of the present methods of calculating dose-rate contributions from air-scattered gamma rays.

Calculations have been carried out and compared with experimental measurements for configurations in which the TSF reactor was in the reactor tank on the reactor tank-crew compartment axis and the detector was inside a crew-compartment mockup. (The GE-ANP crew-compartment mockup was used throughout the experiments.) These calculations were performed for a number of positions of the reactor in the tank and for different thicknesses of shielding material on the side wall of the crew compartment. When the reactor is very near the wall of the reactor

tank, the neutron leakage from the reactor shield is quite large and hence produces a large contribution to the gamma-ray dose rate from neutrons which undergo radiative capture by the nitrogen in the atmosphere. It is obvious that this contribution is especially important when the reactor is close to the tank wall on the side away from the crew compartment, since the direct beam is weak in this case and most of the gamma rays leave the tank at approximately 180 deg from the detector and hence have a small probability of scattering to the detector. On the other hand, as the reactor is moved to greater depths in the reactor tank, the neutrons are attenuated much more rapidly than the gamma rays, and, therefore, the air-capture gamma-ray contribution becomes negligible compared with the air-scattered and direct-beam contributions.

### Dose Rates in Air from Direct Gamma Rays

S. K. Penny

An estimate of the gamma-ray dose rate in air from a direct beam of gamma rays from the TSF reactor as a function of the position of the reactor in the reactor tank was obtained by using a point-to-point attenuation kernel derived from Bulk Shielding Facility (BSF) reactor gamma-ray center-line data. The data were for a BSF reactor fuel element loading that was similar to the TSF reactor loading, and the method used to calculate the kernel was essentially the same as that outlined in an earlier report.<sup>1</sup> The gamma-ray dose rate in the water at a distance  $z$  (Fig. 6.2.1) from the center of the north face of the BSF reactor is given by

$$(1) \quad D(z) = \lambda_c \int_{-a}^a dx \int_{-b}^b dy p(x,y) G(R) ,$$

where

$\lambda_c$  = gamma-ray relaxation length in the core of the BSF reactor,

$a, b$  = half-widths of the north face of the BSF reactor,

$G(R)$  = attenuation kernel for a point source with geometric attenuation included,

$p(x,y)$  = power density on the north face;

$$p(x,y) = p_0(1 - \alpha x^2)(1 - \beta y^2) ,$$

where

$$p_0 = 1.88 \times 10^{-5} \text{ w/cm}^3 \cdot \text{w},$$

$$\alpha = 1.5 \times 10^{-3} \text{ cm}^{-2},$$

$$\beta = 7 \times 10^{-4} \text{ cm}^{-2}.$$

This power distribution was obtained from gold-foil measurements.<sup>2</sup>

If the relaxation length of gamma rays in water,  $\lambda(z)$ , is defined by

$$\lambda(z) = - \frac{D(z)}{dD(z)/dz}$$

<sup>1</sup>E. P. Blizard and T. A. Welton, *The Shielding of Mobile Reactors - II*, ORNL-1133, p 23 (June 30, 1952).

<sup>2</sup>J. L. Meem and E. B. Johnson, *Determination of the Power of the Shield-Testing Reactor. I. Neutron Flux Measurements in the Water-Reflected Reactor*, ORNL-1027 (Aug. 13, 1951).

and it is assumed that

$$G(R) \approx G(z) e^{-(R-z)/\lambda(z)} ,$$

for

$$\frac{x^2 + y^2}{z^2} \ll 1 ,$$

then

$$R - z = z \left\{ 1 + \frac{1}{2} \frac{x^2 + y^2}{z^2} + \dots \right\} - z \approx \frac{x^2 + y^2}{2z} ,$$

and

$$G(R) \approx G(z) e^{-(x^2+y^2)/2z\lambda(z)} .$$

It follows that

$$D(z) = 2\pi G(z) p_0 z \lambda(z) \lambda_c(z) / [2z \lambda(z)] ,$$

where

$$f[2z \lambda(z)] = f(\zeta) = \left\{ \operatorname{erf} \frac{a}{\sqrt{\zeta}} - \alpha \zeta \left[ \frac{1}{2} \operatorname{erf} \left( \frac{a}{\sqrt{\zeta}} \right) - \frac{a}{\sqrt{\pi \zeta}} e^{-a^2/\zeta} \right] \right\} \times \\ \times \left\{ \operatorname{erf} \frac{b}{\sqrt{\zeta}} - \beta \zeta \left[ \frac{1}{2} \operatorname{erf} \left( \frac{b}{\sqrt{\zeta}} \right) - \frac{b}{\sqrt{\pi \zeta}} e^{-b^2/\zeta} \right] \right\} .$$

The relaxation length in the core is given by

$$\frac{1}{\lambda_c} = \frac{0.58}{\lambda(z)} + \frac{0.42}{\lambda_{Al}} ,$$

where 0.58 and 0.42 are volume fractions of water and aluminum, respectively, in the core. The relaxation length for aluminum was estimated in two ways: (1) it was taken to be the mean free path for 4-Mev gamma rays, which yielded  $(1/\lambda_c) = 0.036 + [0.58/\lambda(z)]$ ; and (2) it was assumed that  $\lambda_{Al} = \lambda(z) (N_{H_2O}/N_{Al})$ , where  $N_{H_2O}$  and  $N_{Al}$  are the electron densities in water and aluminum, respectively. These estimates gave

$$\lambda_c = 0.639 \lambda(z) .$$

The attenuation kernel  $G(z)$  for a point source was calculated for both cases. The attenuation kernel  $g(z)$  for a plane collimated source was then obtained from the relation

$$g(z) = 4\pi z^2 G(z) .$$

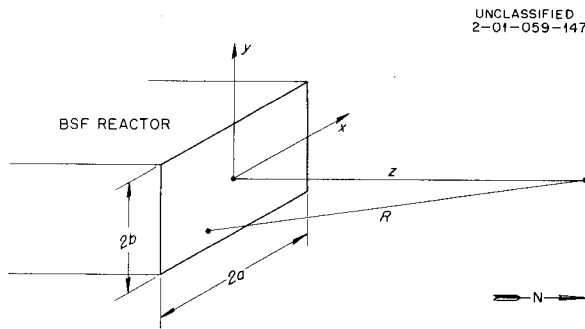
The two cases for the estimate of the value of  $\lambda_c$  resulted in very little difference in the value of  $g(z)$ , and an average value was taken for the computations. These results were supplemented by TSF reactor data in the range where the approximations do not hold, that is, for

$$\frac{a^2 + b^2}{z^2} > 1 .$$

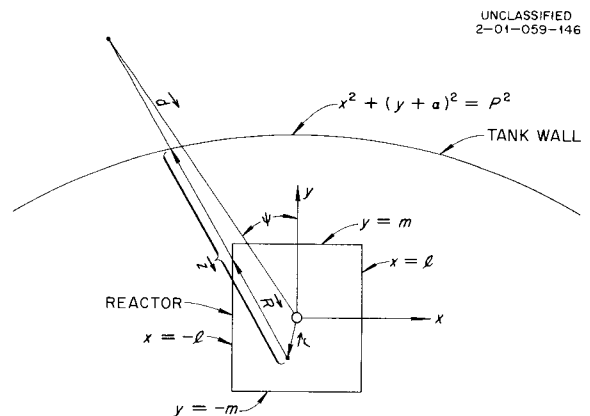
The use of TSF reactor data is justified, since for a separation distance of 64 ft the TSF reactor in its tank appears to be a plane collimated source.

The direct beam from the TSF reactor was calculated on the basis of the following model. The dose rate was calculated in the horizontal median plane of the reactor, with each fuel element considered to be a point source located at the center of the element. Attenuation in the core was taken into account, as was the integrated power over each fuel element, which was used as a weighting factor. The reactor was assumed to be located on a diameter of the 12-ft-dia water-filled tank. For the computations the origin of the coordinate system was taken to be the center of the reactor. The dose rate was computed at a distance of 64 ft from the center of the reactor. The geometry used for the calculations is shown in Fig. 6.2.2, and the terms used for the calculations are defined below:

- $\vec{d}$  = vector distance from the center of the reactor to the point of observation (absolute value, 64 ft; the vector is dependent only on the angle  $\psi$ ),
- $\psi$  = angle between a line joining the center of the reactor and the point of observation and a line joining the centers of the reactor tank and the crew compartment,
- $\vec{r}$  = location vector of the center of a fuel element,
- $\vec{R}$  = path through the reactor,
- $\vec{z}$  = path through the reactor and water in the tank,
- $x^2 + (y + a)^2 = p^2$   
= equation of the surface of the tank,
- $P$  = radius of the tank,
- $a$  = distance between the center of the tank and the center of the reactor.



UNCLASSIFIED  
2-01-059-147



UNCLASSIFIED  
2-01-059-146

Fig. 6.2.1. Geometry for the Calculation of the Attenuation Kernel Used to Determine the Dose Rate in Water Resulting from Direct-Beam Gamma Rays.

Fig. 6.2.2. Geometry for the Calculation of the Dose Rate in Air Resulting from Direct-Beam Gamma-Ray Dose Rates from the TSF Reactor.

ANP PROJECT PROGRESS REPORT

The dose rate at  $\vec{d}$  due to the source at  $\vec{r}$  can be computed if  $R$  and  $z$  are known and the relative integrated power of the fuel element at  $\vec{r}$ , denoted by  $\omega(\vec{r})$ , is known. Hence

$$(2) \quad D(\vec{d}, \vec{r}) = \frac{\omega(\vec{r})}{4\pi|\vec{d} - \vec{r}|^2} g \left\{ z + R \left[ \frac{\lambda_g(z)}{\lambda_{g_c}(z)} - 1 \right] \right\} ,$$

where

$$z = |\vec{z}| ,$$

$$R = |\vec{R}| ,$$

$$\lambda_g(z) = - \frac{g(z)}{dg(z)/dz} ,$$

$$\lambda_{g_c} = 0.639 \lambda_g(z) .$$

It may be observed that the argument of  $g$  is the total water path length plus the equivalent water path length of the core.

The total dose rate at  $\vec{d}$  is given by

$$D(\vec{d}) = \sum_{\vec{r}} D(\vec{d}, \vec{r}) ,$$

and Table 6.2.1 lists values of  $D(\vec{d})$  as a function of  $\psi$  for various values of  $\rho$ , the distance along the reactor center line from the face of the reactor to the reactor tank wall ( $\rho = P - a - m$ , where  $m$  represents the half-width of the reactor). The values given in Table 6.2.1 have been normalized to  $D(\vec{d}) = 1$  at  $\psi = 0$  deg.

In order to compare the results with TSF data,  $D(\vec{d})$  was computed<sup>3</sup> as a function of  $\rho$  and  $\theta$ , the angle between a line joining the center of the reactor tank and the point of observation and

<sup>3</sup>This calculation was performed with the assistance of C. A. Goetz, R. M. Davis, F. L. Keller, and D. K. Trubey.

TABLE 6.2.1. NORMALIZED, CALCULATED, DIRECT-BEAM GAMMA-RAY DOSE RATES IN AIR 64 ft FROM THE CENTER OF THE TSF REACTOR FOR VARIOUS VALUES OF  $\rho$  AND  $\psi$

$\rho$ (cm)	$D(\vec{d})$				
	$\psi = 0$ deg	$\psi = 50.2$ deg	$\psi = 90$ deg	$\psi = 129$ deg	$\psi = 180$ deg
16	1.00	0.863	$7.62 \times 10^{-2}$	$7.34 \times 10^{-4}$	$1.98 \times 10^{-4}$
30	1.00	0.681	$7.23 \times 10^{-2}$	$1.43 \times 10^{-3}$	$4.60 \times 10^{-4}$
45	1.00	0.704	$7.69 \times 10^{-2}$	$2.96 \times 10^{-3}$	$1.19 \times 10^{-3}$
60	1.00	0.703	0.108	$6.64 \times 10^{-3}$	$3.10 \times 10^{-3}$
90	1.00	0.706	0.185	$3.00 \times 10^{-2}$	$1.87 \times 10^{-2}$
120	1.00	0.806	0.369	$1.43 \times 10^{-1}$	$1.11 \times 10^{-1}$
156	1.00				0.870

a line joining the centers of the reactor tank and the crew compartment. The resulting dose rates  $D_c(\rho)$  were normalized to TSF reactor experimental curves at  $\theta = 0$  deg. The normalized curves, shown in Fig. 6.2.3, fit the experimental curves<sup>4</sup> very well in the region  $0 \leq \theta \leq 60$  deg. At larger angles the calculated curves are lower than the measured curves. This result is in agreement with the fact that the fraction of the measured dose rate which is contributed by air-scattered gamma rays increases with increasing angle.

### Dose Rates in the Crew Compartment from Direct Gamma Rays

R. M. Davis<sup>5</sup>

F. L. Keller

W. R. Champion<sup>6</sup>

Calculations were made of the dose rate at the center of the G-E crew compartment from the direct gamma rays from the TSF reactor that pass through the rear lead plug. (A sketch of the G-E crew compartment is shown in Fig. 6.2.6 of the following section.) The incident flux, which was taken from the preceding section, was assumed to be normal to the rear face of the crew compartment.

The following equation was used to calculate the direct-beam dose rates at the center of the crew compartment:

$$(3) \quad D_1(\rho) = \frac{D_c(\rho)}{D_s(\rho)} \int_{E_0=0}^{\infty} N(E_0, \rho) \exp \left[ -\sum_x \mu_x(E_0) t_x \right] B_r^{Pb} \left[ \sum_x \mu_x(E_0) t_x \right] K(E_0) dE_0,$$

where

$N(E_0, \rho)$  = relative number of photons of energy  $E_0$  (Mev) per unit energy interval per square centimeter per second incident on the rear face of the crew compartment for a given reactor shield thickness,  $\rho$  (see Table 6.2.2),<sup>7</sup>

$D_s(\rho)$  = relative calculated dose rate in air based on the spectrum used to obtain  $N(E_0, \rho)$  (see Table 6.2.3),

$D_c(\rho)$  = calculated dose rate (mr/hr·w) in air at the rear of the crew compartment, as determined in the preceding section (see Fig. 6.2.3),

$\mu_x(E_0)$  = total absorption coefficient in any material  $x$  for gamma-ray energy  $E_0$ ,

$t_x$  = thickness of material  $x$ , as given in Table 6.2.4,

$x$  = any of the materials (water, lead, aluminum, or iron) in the rear plug,

$$\sum_x \mu_x(E_0) t_x = \left[ \mu_{Pb}(E_0) t_{Pb} + \mu_{H_2O}(E_0) t_{H_2O} + \mu_{Al}(E_0) t_{Al} + \mu_{Fe}(E_0) t_{Fe} \right],$$

<sup>4</sup>F. N. Watson, *ANP Quar. Prog. Rep. March 10, 1956*, ORNL-2061, Part IV, Figs. 15.7 and 15.8, p 12-13.

<sup>5</sup>The Glenn L. Martin Co.

<sup>6</sup>Lockheed Aircraft Corp.

<sup>7</sup>G. J. Rausa and F. N. Watson, *ANP Quar. Prog. Rep. June 10, 1956*, ORNL-2106, Part VI, p 8-17.

ANP PROJECT PROGRESS REPORT

$B_r^{Pb} \left[ \sum_x \mu_x(E_0) t_x \right]$  = plane monodirectional dose buildup factor in lead for total number of mean free paths in rear shield (see discussion below and Table 6.2.5),

$K(E_0)$  = number flux-to-dose rate conversion factor.

The buildup factors,  $B_r$ , used in the calculations were selected from the plane monodirectional dose buildup factors for lead<sup>8</sup> for the total number of mean free paths presented to the

<sup>8</sup>J. Moteff, *Miscellaneous Data for Shielding Calculations*, APEX-176 (Dec. 1, 1954).

TABLE 6.2.2. RELATIVE NUMBER OF DIRECT-BEAM PHOTONS OF ENERGY  $E_0$  (IN AIR) FOR VARIOUS REACTOR WATER SHIELD THICKNESSES

$E_0$ (Mev)	$N(E_0, \rho)$			
	$\rho = 25$ cm	$\rho = 40$ cm	$\rho = 60$ cm	$\rho = 100$ cm
0.25	50	24.5	17.0	1.1
0.50	50	24.5	17.0	1.4
1.0	50	24.5	17.0	1.8
1.5	50	24.5	17.0	2.3
2.0	50	24.5	17.0	2.7
2.5	50	24.5	16.0	2.9
3.0	50	24.5	15.0	2.8
3.5	29	19.0	9.0	2.15
4.0	17	9.9	5.8	1.4
4.5	11.7	6.2	3.8	1.0
5.0	6.6	3.8	2.5	0.70
5.5	2.4	2.0	1.2	0.46
6.0	0.94	1.2	0.84	0.38
6.5	2.2	2.0	1.2	0.49
7.0	4.9	3.05	1.6	0.65
7.5	3.0	1.70	1.0	0.50
8.0	1.02	0.58	0.53	0.15
8.5	0.33	0.21	0.12	0.03
9.0	0.09	0.06	0.023	0.009

TABLE 6.2.3. GAMMA-RAY DOSE RATES IN AIR

$\rho$ (cm)	$D_s(\rho)$ (mr/hr) <sup>a</sup>	Dose Rates at Rear of Crew Compartment <sup>b</sup> (mr/hr·w)	
		Measured	Calculated with Absolute Spectrum <sup>c</sup>
25	$6.46 \times 10^{-1}$	2.5	1.882
40	$3.52 \times 10^{-1}$	1.26	1.007
60	$2.16 \times 10^{-1}$	$5.9 \times 10^{-1}$	$6.18 \times 10^{-1}$
100	$4.57 \times 10^{-2}$	$1.43 \times 10^{-1}$	$1.26 \times 10^{-1}$

<sup>a</sup>Relative dose rates used for normalization only.

<sup>b</sup>These dose rates are not used in the calculation and are included here only for comparison.

<sup>c</sup>Attenuation by 100 ft of air considered.

gamma rays by the lead, water, and structure of the crew-compartment rear plug. Lead buildup factors only were chosen, since lead is the last material that the gamma rays "see" and accounts for about 65% of the total number of mean free paths traversed. More accurate buildup factors for slabs of finite thicknesses of water and lead are currently being calculated, but sufficient data were not available for this study.

The buildup factors were calculated for gamma-ray energies of 0.5, 1.0, 3.0, and 6.0 Mev (Table 6.2.5), and a plot of the buildup factors as a function of energy was made (Fig. 6.2.4). This plot was then used in Eq. 3 for calculating the gamma-ray attenuations.

The resulting calculated dose rates at the center of the crew compartment obtained for the cases of  $\theta = 0$  deg and  $\rho = 25, 40, 60,$  and  $100$  cm are shown in Fig. 6.2.5 ( $\theta$  and  $\rho$  were defined in the preceding section). This represents 8 to 11% of the total dose rate measured in the crew compartment when only water was present on the sides of the crew compartment. It represents 55 to 75% of the total dose rate measured when both water and lead were present on the sides. If it is assumed that the spectrum for  $\rho = 100$  cm can be used for reactor water shield thicknesses greater than 100 cm, the curve labeled  $\theta = 180$  deg in Fig. 6.2.5 is obtained.

#### Dose Rates in the Crew Compartment from Direct Gamma Rays Scattered in the Crew-Compartment Side Shielding

R. M. Davis

F. L. Keller

W. R. Champion

A calculation was made of the contribution to the dose rate at the center of the G-E crew compartment (Fig. 6.2.6) from direct-beam gamma rays which strike the rear of the crew compartment in the region outside the area of the lead plug and then scatter into the detector from the water side shield. The Klein-Nishina differential scattering cross sections were used for the calculation, which was based on single scattering and took into account energy degradation and attenuation on both legs of the path.

Dose rates were calculated for three shielding geometries. For case I the crew-compartment sides were shielded with 14.4 in. of water only. For case II the sides had the water shield plus a lead shield with a staggered thickness ( $\frac{5}{8}$  in. at rear,  $\frac{1}{4}$  in. at front). For case III the sides had the water and staggered lead shields plus an additional  $\frac{1}{4}$ -in.-thick layer of lead. In all cases the rear plug was full of water and the 5-in.-thick lead end plug was in place.

The dose rates were calculated by the following formula, in which it was assumed that a unit monodirectional flux of 1 photon/cm<sup>2</sup>·sec of energy  $E_0$  was incident upon the rear face of the crew compartment parallel to the reactor-crew compartment axis:

$$(4) \quad D(E_0) = 2\pi n e^{-\mu_{H_2O}(E_0)l} \int_{\beta=\beta_0}^{\pi-\beta_0} \int_{r=a/\sin\beta}^{b/\sin\beta} e^{-\mu'_{H_2O}(E_0,E,\beta)r} \times \\ \times e^{\mu_{H_2O}(E_0)(a/\sin\beta)} e^{-\mu_{Pb}(E)[t_{Pb}(\beta)/\sin\beta]} K(E) \left( \frac{d\sigma}{d\Omega} \right)_{\beta} \sin\beta \, d\beta \, dr .$$

UNCLASSIFIED  
2-01-059-152

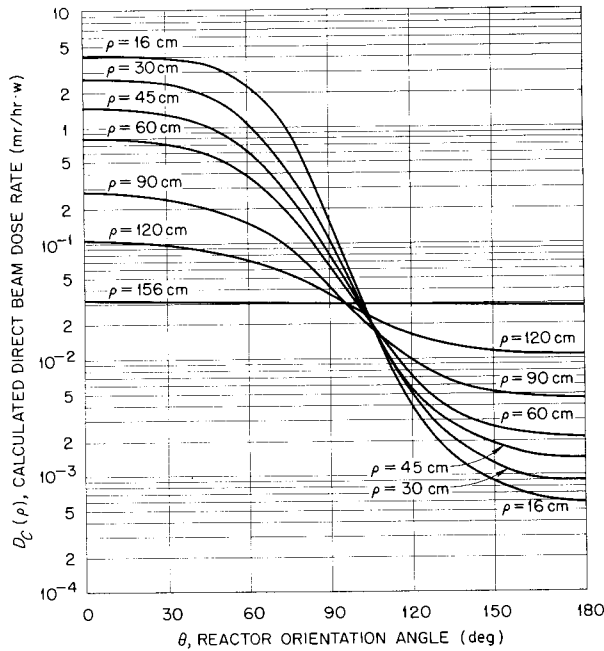


Fig. 6.2.3. Calculated Direct-Beam Gamma-Ray Dose Rates in Air 64 ft from the Center of the TSF Reactor.

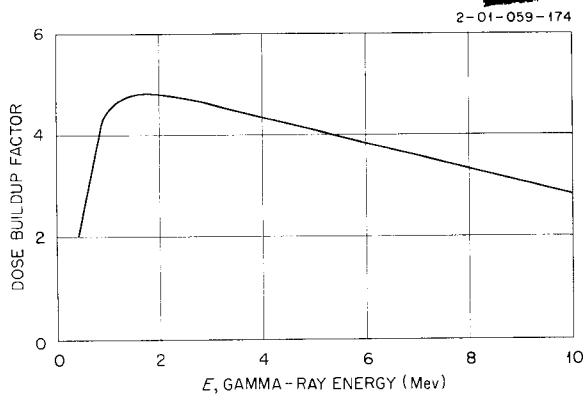


Fig. 6.2.4. Gamma-Ray Dose Rate Buildup Factors for Rear Plug of G-E Crew Compartment as a Function of Photon Energy.

TABLE 6.2.4. THICKNESSES OF SHIELD MATERIALS ON THE REAR FACE OF THE CREW COMPARTMENT

Material	Thickness (cm)
Lead	12.70
Water	73.03
Aluminum	2.54
Iron	0.953

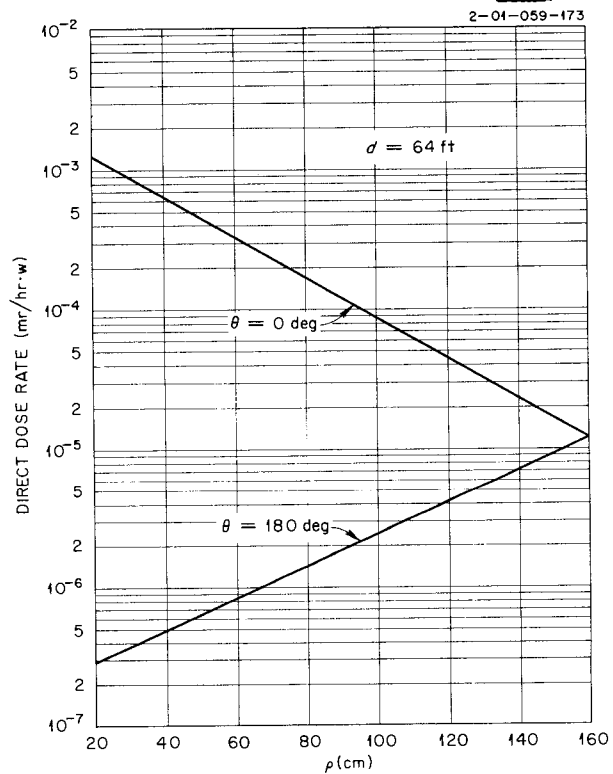


Fig. 6.2.5. Calculated Dose Rates at the Center of the G-E Crew Compartment Resulting from Direct-Beam Gamma Rays from the TSF Reactor ( $\theta = 0$  and  $180$  deg).

When integrated over  $r$ , Eq. 4 becomes

$$(5) \quad 2\pi n e^{-\mu_{H_2O}(E_0)l} \int_{\beta_0}^{\pi-\beta_0} e^{\mu_{H_2O}(E_0) a \cot \beta - \mu_{Pb}(E) [t_{Pb}(\beta)/\sin \beta]} \times \\ \times \left\{ 1 - e^{\mu'_{H_2O}(E_0, E, \beta) [(a-b)/\sin \beta]} \right\} \frac{K(E) (d\sigma/d\Omega)_{\beta} \sin \beta d\beta}{\mu'_{H_2O}(E_0, E, \beta)}$$

TABLE 6.2.5. PLANE MONODIRECTIONAL DOSE BUILDUP FACTORS USED FOR PHOTONS OF VARIOUS ENERGIES IN SHIELD MATERIALS ON REAR FACE OF CREW COMPARTMENT

$E_0$ (Mev)	$\mu_{Pb} t_{Pb}$	$\mu_{H_2O} t_{H_2O}$	$\mu_{Al} t_{Al}$	$\mu_{Fe} t_{Fe}$	$\sum_x \mu_x t_x$	$B_r^{Pb} \left( \sum_x \mu_x t_x \right)$
0.5	22.86	7.01	0.635	0.643	31.15	2.40
1.0	10.16	5.11	0.419	0.438	16.13	4.42
3.0	5.97	2.86	0.239	0.257	9.33	4.60
6.0	6.33	2.04	0.183	0.219	8.77	3.85

2-01-056-3-T24-81

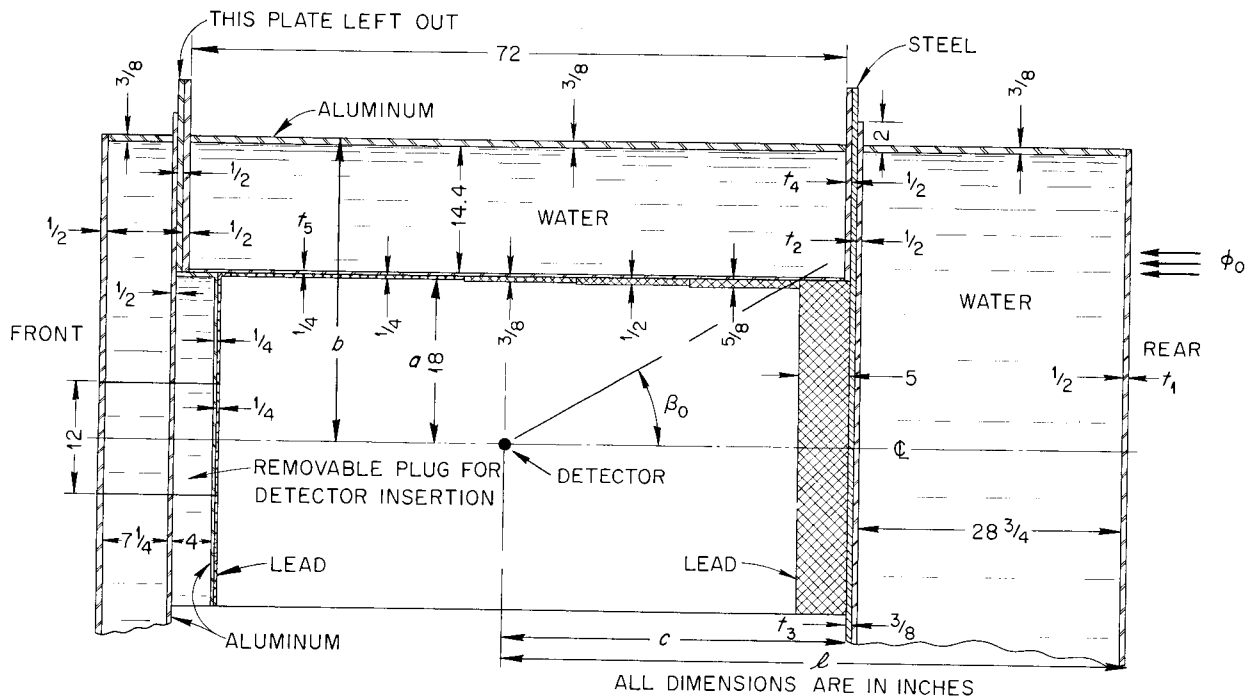


Fig. 6.2.6. Schematic Diagram of the GE-ANP Crew Compartment.

where

- $\beta_0$  = half-angle subtended at the detector by the lead plug of the crew-compartment shield (Fig. 6.2.6),  
 $n$  = electron density of water (electrons/cm<sup>3</sup>),  
 $E_0$  = energy of the incident direct-beam gamma rays,  
 $E$  = energy of the gamma rays after being scattered at an angle  $\beta$ ,  
 $l$  = distance from rear of G-E crew compartment to detector (cm),  
 $\mu'_{H_2O}(E_0, E, \beta) = \mu_{H_2O}(E) - \mu_{H_2O}(E_0) \cos \beta$ ,  
 $\mu_{H_2O}(E)$  = total absorption coefficient in water for photon of energy  $E$ ,  
 $a$  = inside radius of crew compartment (cm),  
 $b$  = outside radius of crew compartment (cm),  
 $K(E)$  = number flux-to-dose rate conversion factor for photons of energy  $E$ ,  
 $(d\sigma/d\Omega)_\beta$  = Klein-Nishina differential scattering cross section (cm<sup>2</sup>/steradian-electron),  
 $\beta$  = angle at which photon is scattered into detector as measured from reactor-crew compartment axis,  
 $t_{Pb}(\beta)$  = thickness of lead at angle  $\beta$  (cm),  
 $\mu_{Pb}(E)$  = total absorption coefficient of lead for photons of energy  $E$ ,  
 $r'$  = distance from scattering center to detector (cm).

For the formula above, the structure is considered to be water. From Fig. 6.2.6 it may be seen, however, that there is an appreciable amount of iron and aluminum structure between the side water shield and the rear plug in addition to the structural aluminum in the outside container walls. Corrections must be made for the greater attenuation properties of the structure. Thus the following formula was used to obtain a factor,  $C(\beta)$ , which could be used to correct the dose-rate contribution at each angle  $\beta$ :

$$(6) \quad C(\beta) = A_1(E_0) \left[ f_1(\beta) A_2(E_0) + f_2(\beta) A_3(E) \right] A_4(E) ,$$

where

$$A_1(E_0) = \exp \left\{ -t_1 \left[ \mu_{Al}(E_0) - \mu_{H_2O}(E_0) \right] \right\} ,$$

$$A_2(E_0) = \exp \left\{ -(t_2 + t_4) \left[ \mu_{Al}(E_0) - \mu_{H_2O}(E_0) \right] - t_3 \left[ \mu_{Fe}(E_0) - \mu_{H_2O}(E_0) \right] \right\} ,$$

$$A_3(E) = \exp \left\{ -\frac{t_2 + t_4}{\cos \beta} \left[ \mu_{Al}(E) - \mu_{H_2O}(E) \right] - \frac{t_3}{\cos \beta} \left[ \mu_{Fe}(E) - \mu_{H_2O}(E) \right] \right\} ,$$

$$A_4(E) = \exp \left\{ -\frac{t_5}{\sin \beta} \left[ \mu_{Al}(E) - \mu_{H_2O}(E) \right] \right\} ,$$

$f_1(\beta)$  = fraction of dose rate in Eq. 4 at angle  $\beta$  arising from scattering centers in the side water shield,

$f_2(\beta)$  = fraction of dose rate in Eq. 4 at angle  $\beta$  arising from scattering centers in the water of the rear plug,

and  $t_1, t_2, t_3, t_4, t_5$  are thicknesses, in centimeters, of the crew-compartment structure as shown in Fig. 6.2.6.

From Eq. 4 it can be seen that the dose-rate contribution at a given angle  $\beta$  varies with  $r$  as  $e^{-\mu' r}$ . Therefore

$$(7) \quad f_1(\beta) = \frac{\int_{a/\sin \beta}^{c/\cos \beta} e^{-\mu' r} dr}{\int_{a/\sin \beta}^{b/\sin \beta} e^{-\mu' r} dr} = \frac{e^{-\mu' c/\cos \beta} - e^{-\mu' a/\sin \beta}}{e^{-\mu' b/\sin \beta} - e^{-\mu' a/\sin \beta}},$$

and

$$f_2(\beta) = 1 - f_1(\beta),$$

where  $c$  is the distance in centimeters from the inside surface of the rear water plug to the detector, as shown in Fig. 6.2.6. No correction was made for the effect upon the scattering of the greater electron density of the structure, since one such correction was computed and found to be less than 5% of the total dose in the crew compartment.

Dose rates were calculated for the three shielding geometries described above for 6-, 3-, and 1.5-Mev incident photons. The results are plotted in Fig. 6.2.7.

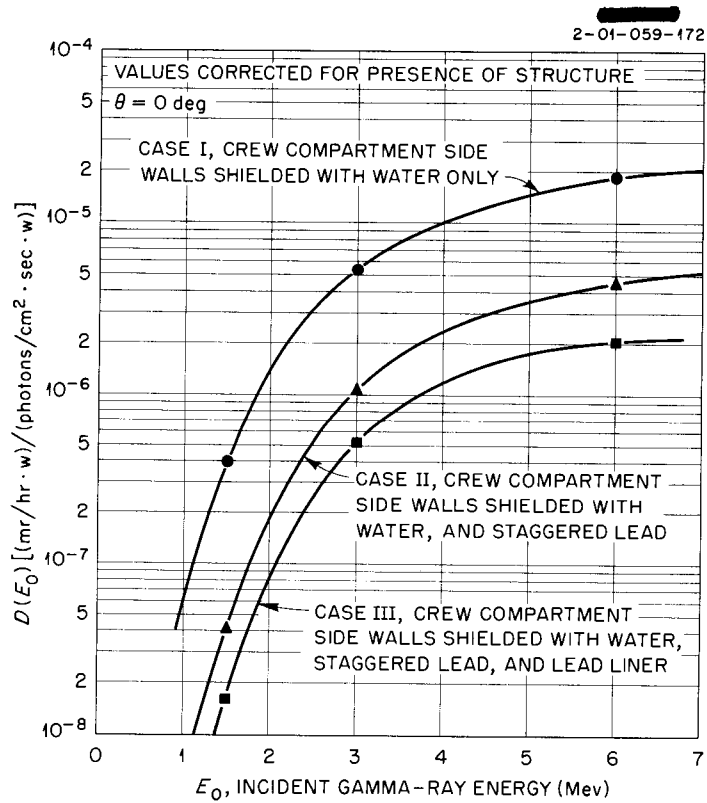


Fig. 6.2.7. Calculated Dose Rates at the Center of the G-E Crew Compartment Resulting from TSF Reactor Direct-Beam Gamma Rays of Incident Energy  $E_0$  That Are Scattered in the Water of the Crew-Compartment Side Walls (Cases I, II, and III;  $\theta = 0 \text{ deg}$ ).

In the next step of the calculation the measured TSF reactor gamma-ray energy spectrum<sup>7</sup> was introduced by using the following formula:

$$(8) \quad D_2(\rho) = \frac{D_c(\rho)}{D_s(\rho)} \int_{E_0=0}^{\infty} D(E_0) N(E_0, \rho) dE_0 ,$$

where the definitions of  $N(E_0, \rho)$ ,  $D_c(\rho)$ , and  $D_s(\rho)$  are the same as those given for Eq. 3, and  $D(E_0)$  is calculated by using Eq. 4.

The results of this calculation, which was performed for both  $\theta = 0$  deg and  $\theta = 180$  deg and for  $\rho = 25, 40, 60,$  and  $100$  cm, are shown in Table 6.2.6. For the  $\theta = 180$ -deg cases, the spectrum for  $\rho = 100$  cm was assumed. In general, the calculated dose rates resulting from the direct beam scattered in the water shield represent 20 to 40% of the total measured dose rates for cases I and III. There are no experimental results to check case II.

TABLE 6.2.6. CALCULATED GAMMA-RAY DOSE RATES IN THE CENTER OF THE G-E CREW COMPARTMENT RESULTING FROM DIRECT GAMMA RAYS SCATTERED IN THE WATER SIDE SHIELDING - CALCULATION BASED ON THE MEASURED SPECTRUM

Configuration	$D_2(\rho)$ (mr/hr·w)			
	$\rho = 25$ cm	$\rho = 40$ cm	$\rho = 60$ cm	$\rho = 100$ cm
$\theta = 0$ deg				
Case I	$3.71 \times 10^{-3}$	$2.21 \times 10^{-3}$	$8.9 \times 10^{-4}$	$3.15 \times 10^{-4}$
Case II	$7.84 \times 10^{-4}$	$4.77 \times 10^{-4}$	$2.12 \times 10^{-4}$	$7.03 \times 10^{-5}$
Case III	$3.75 \times 10^{-4}$	$2.07 \times 10^{-4}$	$1.01 \times 10^{-4}$	$3.34 \times 10^{-5}$
$\theta = 180$ deg				
Case I	$1.20 \times 10^{-6}$	$1.75 \times 10^{-6}$	$3.0 \times 10^{-6}$	$8.55 \times 10^{-6}$
Case II	$2.68 \times 10^{-7}$	$3.91 \times 10^{-7}$	$6.7 \times 10^{-7}$	$1.91 \times 10^{-6}$
Case III	$1.27 \times 10^{-7}$	$1.855 \times 10^{-7}$	$3.18 \times 10^{-7}$	$9.07 \times 10^{-7}$

Dose Rates in the Crew Compartment from Air-Scattered Gamma Rays

R. M. Davis

A calculation of the dose rate at the center of the crew compartment resulting from air-scattered gamma rays which enter the side of the crew shield was performed by applying the single-scattering theory<sup>9</sup> to the normalized direct-beam angular source strengths discussed in a preceding section. (The single-scattering theory was used since the data necessary for a more refined calculation, incorporating multiple scattering, are not yet available.) Two calculational methods were used. In the first the measured TSF reactor gamma-ray energy spectrum<sup>7</sup> was applied, while in the second a monoenergetic source of  $6mc^2$  gamma rays was assumed.

<sup>9</sup>E. P. Blizard and H. Goldstein (eds.), *Report of the 1953 Summer Shielding Session*, ORNL-1575, p 170 (June 14, 1954).

The comparisons of the results of the two methods are of especial interest because of the current practice of assuming that for the air-scattering calculations the energy of all the gamma rays is  $6mc^2$ .

The calculation was performed for two different crew shield geometries, one having a side shield consisting of water only and the other having a side shield consisting of water and lead (see Fig. 6.2.6). In addition, the air-scattered gamma-ray dose rate in air just outside the rear of the crew compartment was calculated.

The formula used in the calculation was taken from ORNL-1575<sup>9</sup> and was modified in such a manner as to simplify the computations and still retain full use of the existing  $f(\psi)$  curves. (The angle  $\psi$  was defined in a preceding section; see Fig. 6.2.2.) The modified formula, which in no way affects the basic assumptions or limitations of the theory, is as follows:

$$(9) D_3(\rho) = 4\pi \times 10^3 d^2 \frac{1500}{a} D_m(d) \int_{\psi=0}^{\pi} \frac{k(\psi, \rho)}{D_s(\rho)} \int_{E_0=0}^{\infty} E_0 [N(E_0, \rho)]_{\psi} f(\psi, E_0) d\psi dE_0 ,$$

where

$D_m(d)$  = direct-beam dose rate measured in air for  $\theta = 0$  deg at a distance  $d$  from the center of the TSF reactor (mr/hr.w) (the definition of  $\theta$  was given in a preceding section),

$k(\psi, \rho)$  = direct dose rate at  $\psi$  normalized to unity for  $\psi = 0$  deg,

$E_0$  = energy of source photon (Mev),

$N(E_0, \rho)$  = number of photons of energy  $E_0$  leaving the source per second per square centimeter per unit energy interval in direction  $\psi$  (function of water thickness in direction  $\psi$ ),

$D_s(\rho)_{\psi}$  = dose rate resulting from  $[N(E_0, \rho)]_{\psi}$  leaving source in direction  $\psi$  (mr/hr),

$f(\psi, E_0)$  = defined in ORNL-1575,<sup>9</sup>

$a$  = distance from center of TSF reactor to detector (cm),

$1500/a$  = correction factor to convert the  $f(\psi)$  curves from a value at 1500 cm to the value at distance  $a$ ,

$10^3$  = factor to convert from r/hr to mr/hr.

From the above definitions it is clear that the combined parameters  $d^2 D_m(d) k(\psi, \rho)$  represent the angular source strength in mr/hr.w. Caution should be taken to assure that all the parameters used in the formula are chosen properly for the reactor at  $\theta = 180$  deg.

**Utilization of Existing  $f(\psi)$  Curves.** – The  $f(\psi)$  curves presented in ORNL-1575<sup>9</sup> were not directly applicable to the modified formula, since there were no curves to correspond to the exact lead and water thicknesses used on the side of the G-E crew compartment. The correct  $f(\psi)$  values were obtained by interpolation; for the interpolation both the aluminum side walls and the water side shielding were converted to equivalent polyethylene  $[(CH_2)_n, \text{ density} = 0.9 \text{ g/cm}^3]$  thicknesses on the basis of electron density. The results were then plotted as a function

of energy for various values of  $\psi$ . This form was chosen because it is most convenient to perform the energy integration first.

The scope of the  $f(\psi)$  curves presented in ORNL-1575 is such that the calculation of the dose rate was limited to integration over angles less than  $\psi = 100$  deg for the case with water side shielding only on the crew compartment and the integration over angles less than  $\psi = 50$  deg for the case of water and lead side shielding. Therefore dose rates in the crew compartment were calculated only for cases in which the source strength was peaked sharply in the forward direction ( $\theta = 0$  deg). In these cases little error was incurred by this limitation.

Calculations of the dose rate in air at the rear of the crew compartment were made for both the case of  $\theta = 0$  deg and the case of  $\theta = 180$  deg, since the extrapolation of the in-air  $f(\psi)$  curves to larger values of  $\psi$  appeared to be reasonable. The error introduced by extrapolating to a finite value of  $f(\psi)$  at  $\psi = 180$  deg was estimated to be 10% for the worst case, which is for  $\rho = 16$  cm and  $\theta = 180$  deg.<sup>10</sup> This error caused the predicted dose rate to be high.

No attempt was made to correct the calculated dose rate for the attenuation of the rear plug of the crew compartment. The method suggested for this in ORNL-1575 would be applicable to this geometry if the limits of  $\psi$  to  $(\psi + \pi/6)$  were placed on the  $\theta$  integration in the determination of the  $f(\psi)$  curves. For the purposes of this study, however, the time required to revise the  $f(\psi)$  curves with these integration limits was considered to be prohibitive.

**Application of the Measured TSF Reactor Energy Spectrum.** – The direct-beam energy spectra incorporated in this study were measured at the TSF reactor<sup>7</sup> as a function of the water thickness ( $\rho$ ) at the reactor. Tables 6.2.2 and 6.2.3 in a preceding section show the spectra and resulting dose rates in air, respectively.

The energy spectrum chosen for a given angle  $\psi$  was estimated on the basis of the water thickness in that direction from the edge of the reactor to the tank wall. The energy integration was performed first with the use of energy spectra chosen as stated above. Normalization was then made for a given  $\rho$  by the terms  $D_m(d)$ ,  $k(\psi, \rho)$ , and  $D_s(\rho)$  before the  $\psi$  integration was performed. The spectrum for  $\rho = 25$  cm was assumed for any water thickness less than 25 cm, and the spectrum for  $\rho = 100$  cm was assumed for any water thickness greater than 100 cm.

**Determination of Source Strength.** – The single-scattering theory in the calculation assumes a point source with an angular variation in source strength. For this study it was assumed that the direct-beam variations reported in Table 6.2.1 were applicable. These angular variations were used for the necessary values of  $k(\psi, \rho)$ . Measurements made at the TSF at a constant separation distance in various directions indicate that the assumption of sphericity for the TSF reactor is reasonable.

<sup>10</sup>This extrapolation for  $\psi = 180$  deg should go to zero; see D. R. Otis and H. C. Woodsum, *First Semiannual ANP Shielding Information Meeting, May 7–8, 1956, Volume II, ORNL-2115, Paper II-1 (July 2, 1956)*. The fact that it goes to a finite value introduces an estimated error of 10% in this particular calculation.

The values of  $D_m(d)$  were obtained from the measurements made in air at the rear of the G-E crew compartment.<sup>11</sup> This assumes that the measured dose rate is 100% direct beam. The results presented here show that the single air-scattered contribution of the measured dose rate is about 5%. Recent measurements made in air at some distance from the crew compartment show that there is no appreciable contribution to the previously measured dose rate either from gamma rays produced by thermal-neutron captures in the rear plug or from back-scattered gamma rays. The calculation of dose rate in air resulting from gamma rays produced by thermal-neutron captures in air (see following section) indicates that at  $\theta = 0$  deg this contribution to the measured dose rate is also negligible.

**Results and Discussion.** – Dose rates were calculated for two of the shielding configurations described in the previous section (cases I and III) and for a point in space (identified as case A). For all cases calculations were performed for both a source having a broad energy spectrum and for a monoenergetic source of  $6mc^2$  gamma rays:

Case A. – Dose rate in air at rear of G-E crew compartment for  $\theta = 0$  deg and  $\theta = 180$  deg.

Case I. – Dose rate inside G-E crew compartment (Fig. 6.2.6) for  $\theta = 0$  deg; side wall of crew compartment shielded with water only; equivalent plastic shield thickness = 44.5 cm.

Case III. – Dose rate inside G-E crew compartment for  $\theta = 0$  deg; side wall of crew compartment shielded with water, staggered lead, plus a lead liner; equivalent plastic shield thickness = 44.5 cm and average lead thickness = 1.90 cm.

Case A. – The calculation of the dose rate in air was performed primarily to indicate the applicability of the single-scattering theory when used with the existing  $f(\psi)$  curves and known source angular strengths and source energy spectra for predicting dose rates in air. The general conclusion is that the single-scattering theory cannot be used to calculate accurately the air-scattered dose rates in geometries in which the angular source strength is highly peaked away from the detector. This is discussed further in the section entitled "Comparison of the Total Calculated Dose Rate with the Measured Dose Rate."

The effect of assuming a monoenergetic source of  $6mc^2$  photons for in-air calculations as opposed to using the energy spectrum is shown in Figs. 6.2.8 and 6.2.9 for  $\theta = 0$  and 180 deg, respectively. The assumption of  $6mc^2$  as an average energy is quite good for large values of  $\rho$  at both  $\theta = 0$  deg and  $\theta = 180$  deg. This is attributed to the hardening of the spectrum with increasing water thickness. If an average energy is calculated by the equation

$$(10) \quad \overline{E_0}(\rho) = \frac{\int_{E_0=0}^{\infty} E_0 F(E_0) N(E_0, \rho) dE_0}{F(\overline{E_0}) \int_{E_0=0}^{\infty} N(E_0, \rho) dE_0}$$

where  $F(E_0)$  is the energy flux-to-dose rate conversion factor in air, it is found that the average energy changes from 2.0 Mev for  $\rho = 25$  cm to 2.8 Mev for  $\rho = 100$  cm.

<sup>11</sup>F. N. Watson, ANP Quar. Prog. Rep. March 10, 1956, ORNL-2061, Part IV, Fig. 15.3, p 8.

The difference between the dose rate predicted by using the spectrum and the dose rate predicted by using the monoenergetic source is greater at  $\theta = 180$  deg than at  $\theta = 0$  deg. This is attributed to the fact that as  $\psi$  increases, the lower energy gamma rays are weighted more heavily with respect to the higher energy gamma rays. This can be seen in Fig. 6.2.10, where the ratio of  $f(\psi)$  for  $3mc^2$  gamma rays to  $f(\psi)$  for  $6mc^2$  gamma rays is 1.24 at  $\psi = 0$  deg and is 3.57 at  $\psi = 120$  deg. With  $\theta = 180$  deg and relatively small values of  $\rho$ , the major portion of the air-scattered dose rate comes from the gamma rays emerging at approximately  $\psi = 140$  deg.

Cases I and III. - For the calculation of dose rates inside the crew compartment, the low-energy portion of the spectrum becomes less important, since it is rapidly attenuated by the crew-compartment shielding. This is illustrated by cases I and III in Fig. 6.2.8, where a higher dose results from the calculation based on the assumption of a monoenergetic source of  $6mc^2$  than from the calculation based on the spectrum. The effect is more marked in case III, since

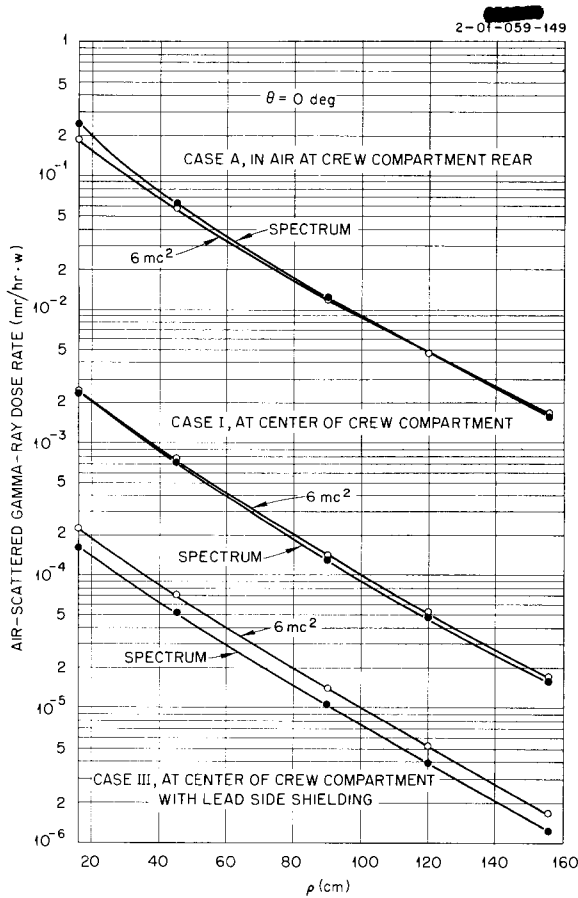


Fig. 6.2.8. Calculated Dose Rates in Air and at the Center of the G-E Crew Compartment Resulting from Air-Scattered Gamma Rays from the TSF Reactor (Cases A, I, and III;  $\theta = 0$  deg).

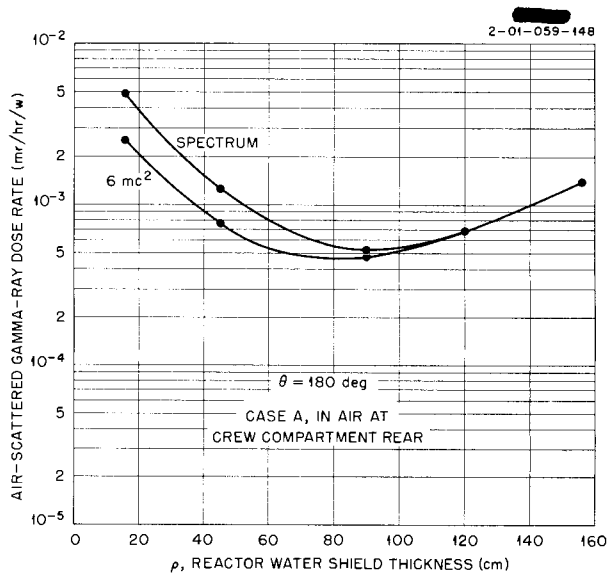


Fig. 6.2.9. Calculated Dose Rates in Air Resulting from Air-Scattered Gamma Rays from the TSF Reactor (Case A,  $\theta = 180$  deg).

the absorption coefficient is a more rapidly rising function in lead, as the energy decreases, than in water. For both cases I and III the curves are essentially parallel throughout the entire range of  $\rho$ , which indicates again that the low-energy portion of the spectrum is less effective inside the crew compartment than outside and that the hardening of the spectrum leaving the reactor tank is less important.

The fact that no  $f(\psi)$  curves exist with which a calculation can be made of the air-scattered contribution to the total dose rate in the crew compartment for  $\theta = 180$  deg precludes an accurate comparison of the total calculated dose rate in the crew compartment with the total measured dose rate for this reactor position. Since for  $\theta = 180$  deg the air-scattered contribution to the measured dose rate is far more important than it is for  $\theta = 0$  deg and since this reactor position in the tank more nearly simulates current shield-shaping trends, a calculation for  $\theta = 180$  deg is needed. Such a calculation would also allow a better determination of the effect of assuming a  $6mc^2$  gamma-ray energy and of the effect of using the single-scattering theory.

The effectiveness of placing lead at the crew compartment is shown by cases I and III. The addition of 1.90 cm of lead attenuated the dose rate from the spectrum by roughly a factor of 13, or 2.56 relaxation lengths.

#### Dose Rates in Air and in the Crew Compartment from Air-Capture Gamma Rays

C. A. Goetz<sup>12</sup>

As a first step in the calculation of the air-capture gamma-ray dose rate at the center of the crew compartment, a calculation was made of the air-capture dose rate at a point in space. The calculation was coded for the Oracle. The code was designed to be general enough to be applicable to any reactor; however, the current primary interest is for the application to the TSF reactor. The results of these machine calculations are presented in a form such that an extension gives an estimate of the air-capture gamma-ray dose rate inside the G-E crew compartment. The dose rates in the crew compartment were calculated for the two shielding geometries designated as case I and case III in the preceding section. (In case I the crew-compartment sides were shielded with water only. In case III the sides were shielded with the water plus a lead layer of staggered thickness plus a lead layer of constant thickness. A schematic diagram of the crew compartment is shown in Fig. 6.2.6 in a preceding section.)

For the in-air dose-rate calculation it was assumed that the thermal-neutron flux was cylindrically symmetric about some axis. This axis, labeled the "axis of symmetry of the thermal-neutron flux," is shown in Fig. 6.2.11. The reactor-detector axis is represented by the line  $d$ . The symbol  $\theta'$  represents the angle between  $d$  and the axis of symmetry; by including this angle in the problem it is possible to calculate the dose rate at points off the axis of symmetry. Thermal-neutron capture occurs in the differential element of volume  $dV$ . This differential volume is located at the point  $(r_1, \theta)$ , where  $r_1$  is the distance from the center of the reactor to

<sup>12</sup>Pratt & Whitney Aircraft.

the point and  $\theta$  is the angle between  $r_1$  and the axis of symmetry. The symbol  $r_2$  represents the distance that a gamma ray produced from thermal-neutron capture in  $dV$  must travel from  $dV$  to the point  $D$  where the detector is located if it makes no collision before reaching the point  $D$ ;  $\beta$  is the angle made by the lines  $r_2$  and  $d$ ; and  $\omega$  is the angle made by the plane defined by the lines  $r_2$  and  $d$  and the plane defined by the axis of symmetry and the line  $d$ .

Since oxygen has a negligible thermal-neutron absorption cross section for the  $(n,\gamma)$  reaction, all the air-capture gamma rays were assumed to be produced in the nitrogen. The microscopic thermal-neutron absorption cross section,  $\sigma_N(n,\gamma)$ , was taken to be equal to 0.1 barn;<sup>13</sup> hence the macroscopic cross section,  $\Sigma_N(n,\gamma)$ , for this reaction was set equal to  $4.19 \times 10^{-6} \text{ cm}^{-1}$ . Kinsey *et al.*<sup>14</sup> have compiled data for the average number,  $P(E)$ , of gamma rays of energy  $E$  emitted by nitrogen per thermal-neutron capture. The values of  $P(E)$  and other energy-dependent parameters employed in the calculation are given in Table 6.2.7. Hence, if  $\phi(r_1, \theta, \rho)$  represents the effective thermal-neutron flux per watt at the point  $(r_1, \theta)$  when the TSF reactor is shielded by water of thickness  $\rho$ , the number,  $N(E)$ , of gamma rays of energy  $E$  produced per second per watt per unit volume in the volume element  $dV$  located at this point is given by

$$(11) \quad N(E) dV = P(E) \Sigma_N \phi(r_1, \theta, \rho) dV .$$

<sup>13</sup>A value of  $0.10 \pm 0.05$  barn is reported by D. J. Hughes and J. A. Harvey, *Neutron Cross Sections*, BNL-325 (July 1, 1955).

<sup>14</sup>G. A. Bartholomew and B. B. Kinsey, *Can. J. Phys.* 31, 49 (1953).

TABLE 6.2.7. NUMERICAL VALUES OF ENERGY-DEPENDENT PARAMETERS EMPLOYED IN CALCULATION OF AIR-CAPTURE GAMMA-RAY DOSE RATE

$E$ (MeV)	$P(E)$	$K(E) \left( \frac{r/\text{hr}}{\text{photons}/\text{cm}^2 \cdot \text{sec}} \right)$	$C(E) \left( \frac{mr/\text{hr}}{\text{photons}/\text{cm}^2 \cdot \text{sec}} \right)$	$m(E)$ ( $\text{cm}^{-1}$ )	$\mu(E)$ ( $\text{cm}^{-1}$ )
10.816	0.192	$1.13 \times 10^{-5}$	$7.23 \times 10^{-10}$	$0.73 \times 10^{-5}$	$2.39 \times 10^{-5}$
9.156	0.0173	$9.92 \times 10^{-6}$	$5.72 \times 10^{-11}$	$0.84 \times 10^{-5}$	$2.54 \times 10^{-5}$
8.278	0.0365	$9.16 \times 10^{-6}$	$1.11 \times 10^{-10}$	$0.93 \times 10^{-5}$	$2.66 \times 10^{-5}$
7.356	0.108	$8.35 \times 10^{-6}$	$3.01 \times 10^{-10}$	$1.07 \times 10^{-5}$	$2.80 \times 10^{-5}$
7.164	0.0365	$8.18 \times 10^{-6}$	$9.94 \times 10^{-11}$	$1.10 \times 10^{-5}$	$2.82 \times 10^{-5}$
6.318	0.172	$7.43 \times 10^{-6}$	$4.26 \times 10^{-10}$	$1.29 \times 10^{-5}$	$2.99 \times 10^{-5}$
5.554	0.287	$6.77 \times 10^{-6}$	$6.46 \times 10^{-10}$	$1.51 \times 10^{-5}$	$3.15 \times 10^{-5}$
5.287	0.440	$6.52 \times 10^{-6}$	$9.55 \times 10^{-10}$	$1.59 \times 10^{-5}$	$3.22 \times 10^{-5}$
4.285	0.153	$5.79 \times 10^{-6}$	$2.95 \times 10^{-10}$	$1.90 \times 10^{-5}$	$3.48 \times 10^{-5}$
4.0	0.197	$5.35 \times 10^{-6}$	$3.51 \times 10^{-10}$	$2.13 \times 10^{-5}$	$3.69 \times 10^{-5}$
3.0	0.050	$4.17 \times 10^{-6}$	$6.97 \times 10^{-11}$	$3.11 \times 10^{-5}$	$4.30 \times 10^{-5}$

Since the capture gamma rays are emitted isotropically from the point of capture, the differential dose rate per watt at  $D$  resulting from gamma rays of energy  $E$  from the volume element  $dV$  is

$$(12) \quad dD(E, d, \theta', \rho) = \frac{P(E) \Sigma_N \phi(r_1, \theta, \rho) B[\mu(E) r_2] e^{-\mu(E) r_2}}{4\pi r_2^2 K(E)} dV ,$$

where

$K(E)$  = number flux-to-dose rate conversion factor for photons of energy  $E$  (see Table 6.2.7),

$B[\mu(E) r_2]$  = dose rate buildup factor in air,

$\mu(E)$  = total gamma-ray absorption coefficient in air (see Table 6.2.7).

If it is assumed that

$$C(E) = \frac{P(E) \Sigma_N}{4\pi K(E)} ,$$

the air-capture gamma-ray dose rate per watt at  $D$  resulting from gamma rays of energy  $E$  is given by

$$(13) \quad D(E, d, \theta', \rho) = C(E) \int_0^\infty \int_0^{2\pi} \int_0^\pi \frac{\phi(r_1, \theta, \rho) B(\mu r_2) e^{-\mu r_2}}{r_2^2} r_2^2 \sin \beta \, d\beta \, d\omega \, dr_2$$

or

$$(14) \quad D(E, d, \theta', \rho) = \int_0^\pi M'(\beta, d, \theta', E, \rho) \, d\beta ,$$

where

$$M'(\beta, E, d, \theta', \rho) = C(E) \sin \beta \int_0^\infty B(\mu r_2) e^{-\mu r_2} \int_0^{2\pi} \phi(r_1, \theta, \rho) \, d\omega \, dr_2 .$$

The total air-capture gamma-ray dose rate per watt is then

$$(15) \quad D(d, \theta', \rho) = \sum_E D(E, d, \theta', \rho) = \sum_E \int_0^\pi M'(\beta, E, d, \theta', \rho) \, d\beta .$$

The quantity  $M'(\beta, E, d, \theta', \rho)$  is of primary interest and was actually calculated. This quantity represents the differential capture gamma-ray dose rate per watt resulting from photons of energy  $E$  arriving at point  $D$  in the conical shell between the angles  $\beta$  and  $\beta + d\beta$ .

The buildup factors for gamma rays in air were obtained from another report.<sup>15</sup> For this calculation it was decided to fit the curves for the buildup factor with the expression  $B[\mu(E) r_2] = 1 + m(E) r_2$ ; it was thus possible to set  $m(E)$  equal to zero to obtain the differential dose rate resulting from the uncollided gamma-ray flux.

The values of  $\phi(r_1, \theta, \rho)$ , the effective thermal-neutron flux surrounding the TSF reactor, used in the calculation were taken from recent TSF experiments. Plots of the flux as a function of the radial distance from the center of the reactor are presented in Fig. 6.2.12 for  $\rho = 45$  cm

<sup>15</sup>L. D. Gates, Jr., and C. Eisenhauer, *Spectral Distribution of Gamma Rays Propagated in Air*, AFSWP No. 502A (Jan. 1954).

UNCLASSIFIED  
2-01-059-171

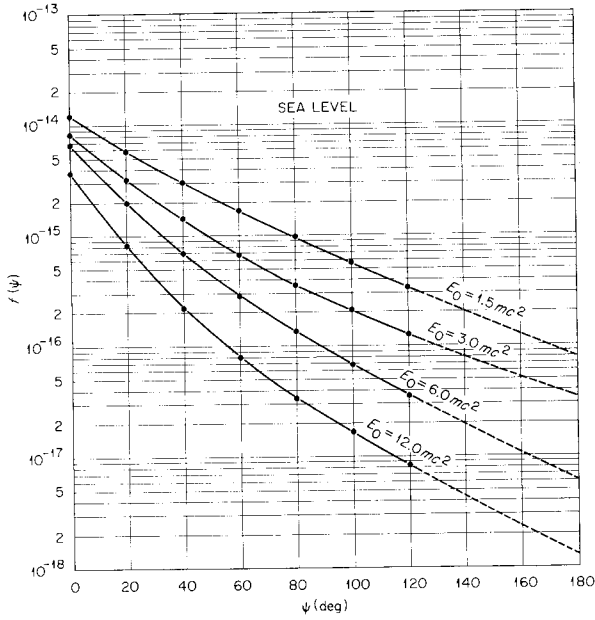


Fig. 6.2.10. The Function  $f(\psi)$  for Several Gamma-Ray Energies and a Point in Air 50 ft from the TSF Reactor.

UNCLASSIFIED  
2-01-059-165

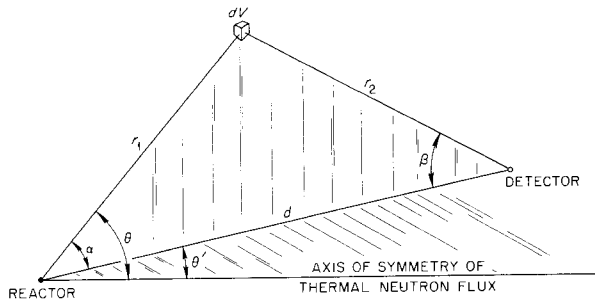


Fig. 6.2.11. Geometry for the Calculation of the Gamma-Ray Dose Rate in Air Resulting from the Air Capture of Thermal Neutrons from the TSF Reactor.

2-01-059-166

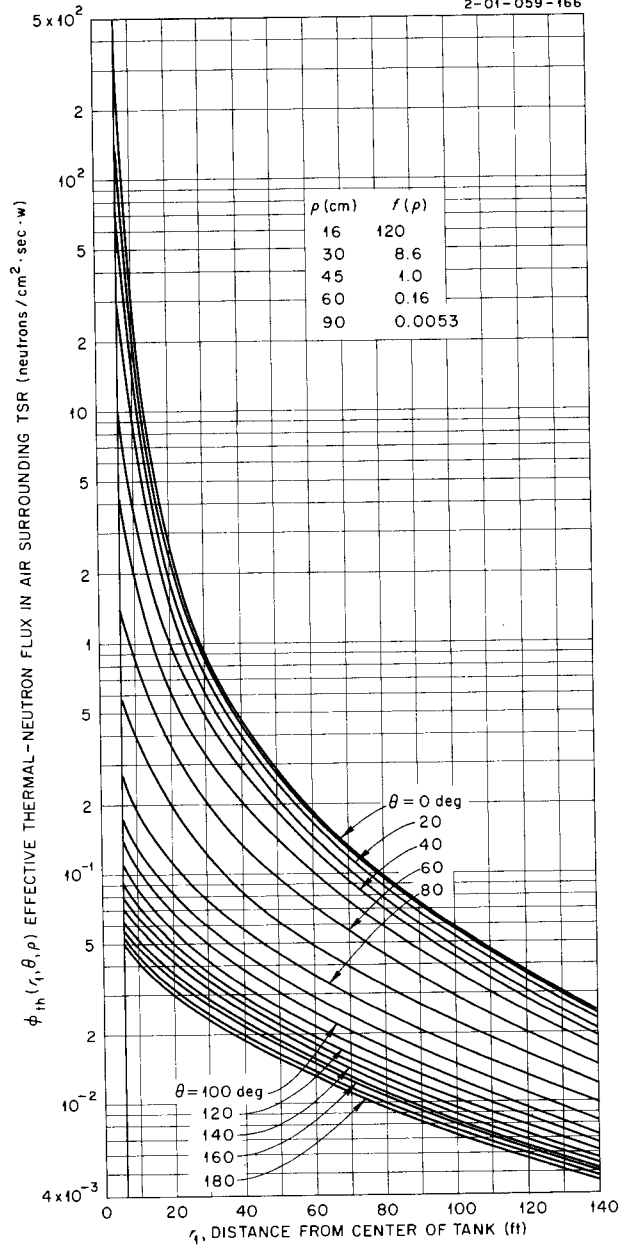


Fig. 6.2.12. Approximate Effective Thermal-Neutron Flux in Air as a Function of Distance from the Center of the TSF Reactor ( $\rho = 45 \text{ cm}$ ).

and for various values of  $\theta$ . Comparison of TSF data for other values of  $\rho$  showed that for  $\rho$  less than 90 cm the angular and radial variation of the thermal-neutron flux is independent of the value of  $\rho$ . Hence, to obtain the air-capture gamma-ray dose rate at a point in space for any other value of  $\rho$ , it is merely necessary to multiply the dose rate for  $\rho = 45$  cm by a specified factor,  $f(\rho)$ , given on Fig. 6.2.13.

The thermal-neutron flux data shown in Fig. 6.2.12, which represents distances out to 140 ft, were stored in the fast memory of the Oracle in tabular form, since they could not be fitted to an expression that could be put into the Oracle. The computer could obtain by interpolation the flux for any value of  $r_1$  less than 140 ft that was not included in the tabulation. For  $r_1$  greater than 140 ft the flux was approximated by the expression

$$\phi_{tb}(r_1, \theta, \rho) = \frac{A(\theta, \rho) e^{-Br_1}}{r_1},$$

where  $B = 8.48 \times 10^{-5} \text{ cm}^{-1}$ . The value for  $B$  was obtained from the slope of the curve of  $r_1 \cdot \phi_{tb}(r_1, 180 \text{ deg})$  in the vicinity of  $r_1$  equal to 140 ft, and it agrees fairly well with the value calculated under the assumption that the diffusion process governs the behavior of the neutrons at large distances from the reactor.

Since

$$r_1 = (r_2^2 + d^2 - 2r_2 d \cos \beta)^{1/2}$$

and

$$\theta = \cos^{-1}(\cos \alpha \cos \theta' + \sin \alpha \sin \theta' \cos \omega),$$

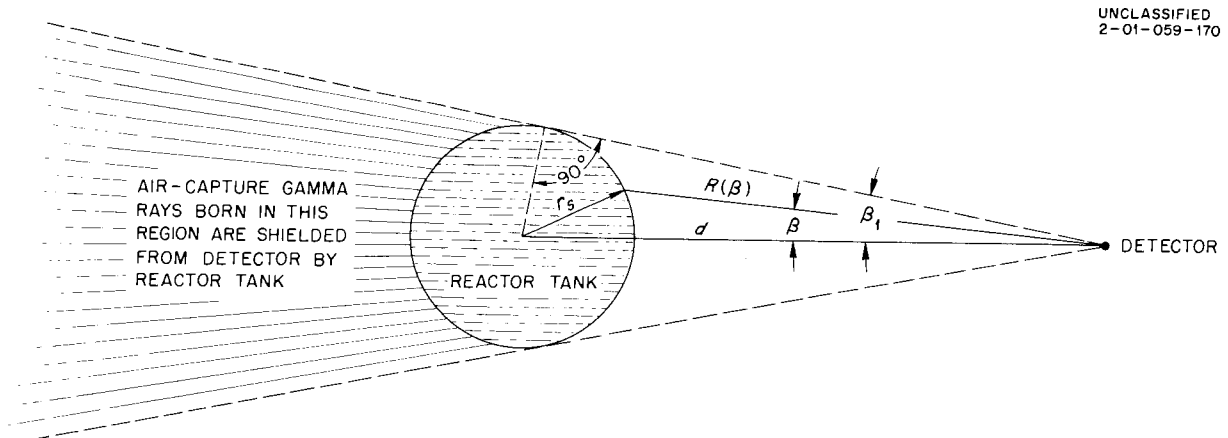


Fig. 6.2.13. Geometry to Take into Account the Interception of Radiation by the TSF Reactor Tank (Used in Calculation of Air-Capture Gamma-Ray Dose Rate).

the final form of the equation for  $M'(\beta, E, d, \theta', \rho)$  is

$$M'(\beta, E, d, \theta', \rho) = C(E) \sin \beta \int_0^{R(\beta)} \int_0^{2\pi} [1 + m(E) r_2] e^{-\mu(E) r_2} \times \\ \times \phi \left[ \left( r_2^2 + d^2 - 2r_2 d \cos \beta \right)^{1/2}, \cos^{-1} (\cos \alpha \cos \theta' + \sin \alpha \sin \theta' \cos \omega), \rho \right] d\omega dr_2 ,$$

where (see Fig. 6.2.13)

$$R(\beta) = \begin{cases} \text{a large number,} & \text{for } \beta \geq \beta_1 , \\ d \cos \beta - (r_s^2 - d^2 \sin^2 \beta)^{1/2}, & \text{for } \beta < \beta_1 , \end{cases}$$

$r_s$  = radius of reactor shield (that is, radius of TSF reactor tank, which is 6 ft),

$\beta_1$  = half-angle subtended by reactor at detector.

Only a few cases have been computed at this time. Figures 6.2.14 through 6.2.16 show representative curves of  $M'(\beta, E, d, \theta', \rho)$  as a function of  $\beta$  for several choices of parameters. In addition to the points computed by the Oracle, several points were computed by hand.<sup>16</sup> All points were in good agreement.

<sup>16</sup>Hand computations were performed with the assistance of L. Bowman and J. Hilgeman, Wright Air Development Center; A. Futterer, Pratt & Whitney Aircraft; V. J. Sholund, Lockheed Aircraft Corp.; and S. K. Penny and D. K. Trubey, ORNL.

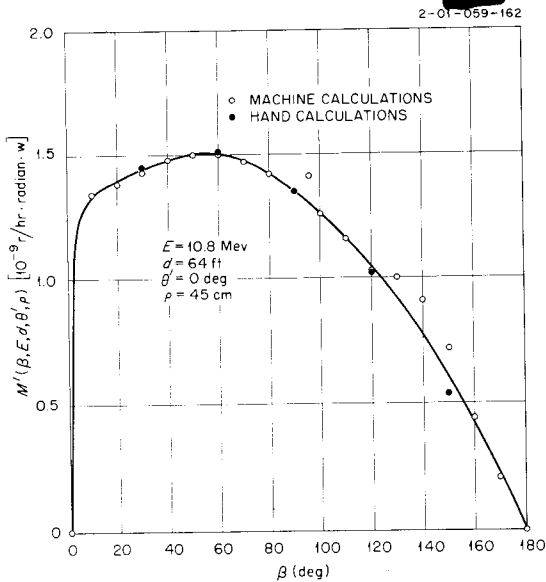


Fig. 6.2.14. Differential Air-Capture Gamma-Ray Dose Rates in Air Surrounding the TSF Reactor for 10.8-Mev Photons and  $\theta' = 0$  deg.

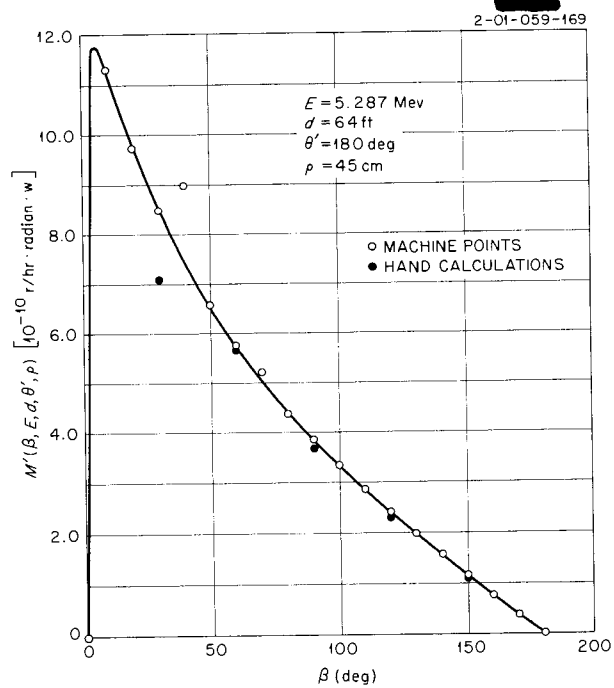
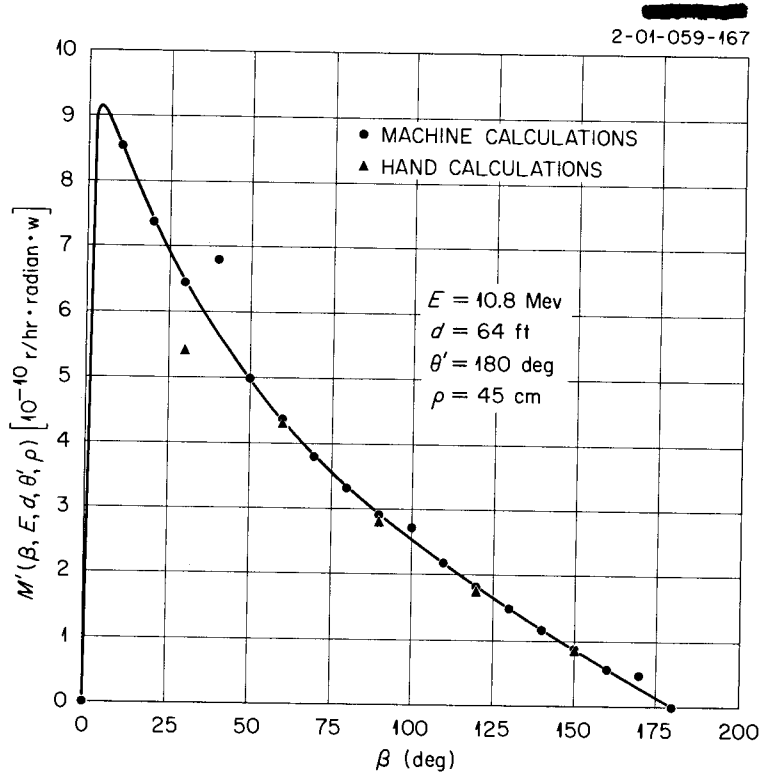


Fig. 6.2.15. Differential Air-Capture Gamma-Ray Dose Rates in Air Surrounding the TSF Reactor for 5.287-Mev Photons and  $\theta' = 180$  deg.



**Fig. 6.2.16. Differential Air-Capture Gamma-Ray Dose Rates in Air Surrounding the TSF Reactor for 10.8-Mev Photons and  $\theta' = 180 \text{ deg}$ .**

If the point  $D$  in Fig. 6.2.13 is considered to be the center of a crew compartment (the G-E crew compartment in this case), the dose rate inside the crew compartment can be determined by weighting  $M'(\beta, E, d, \theta', \rho)$  by the attenuation and buildup factors corresponding to the slant thickness determined by the angle of penetration  $\beta$  (see Fig. 6.2.17). Hence the dose rate inside a crew compartment is given by

$$\begin{aligned}
 D(d, \theta', \rho) &= \sum_E \int_0^\pi M'(\beta, E, d, \theta', \rho) e^{-\mu'(E) t(\beta)} B'[\mu'(E) t(\beta)] d\beta \\
 &= \sum_E \int_0^\pi G'(\beta, E, d, \theta', \rho) d\beta \\
 &= \int_0^\pi G(\beta, d, \theta', \rho) d\beta,
 \end{aligned}$$

where

$t(\beta)$  = slant thickness of the crew-compartment shielding material at the angle  $\beta$ ,  
 $\mu'$  = total gamma-ray absorption coefficient of the crew-compartment shielding material,

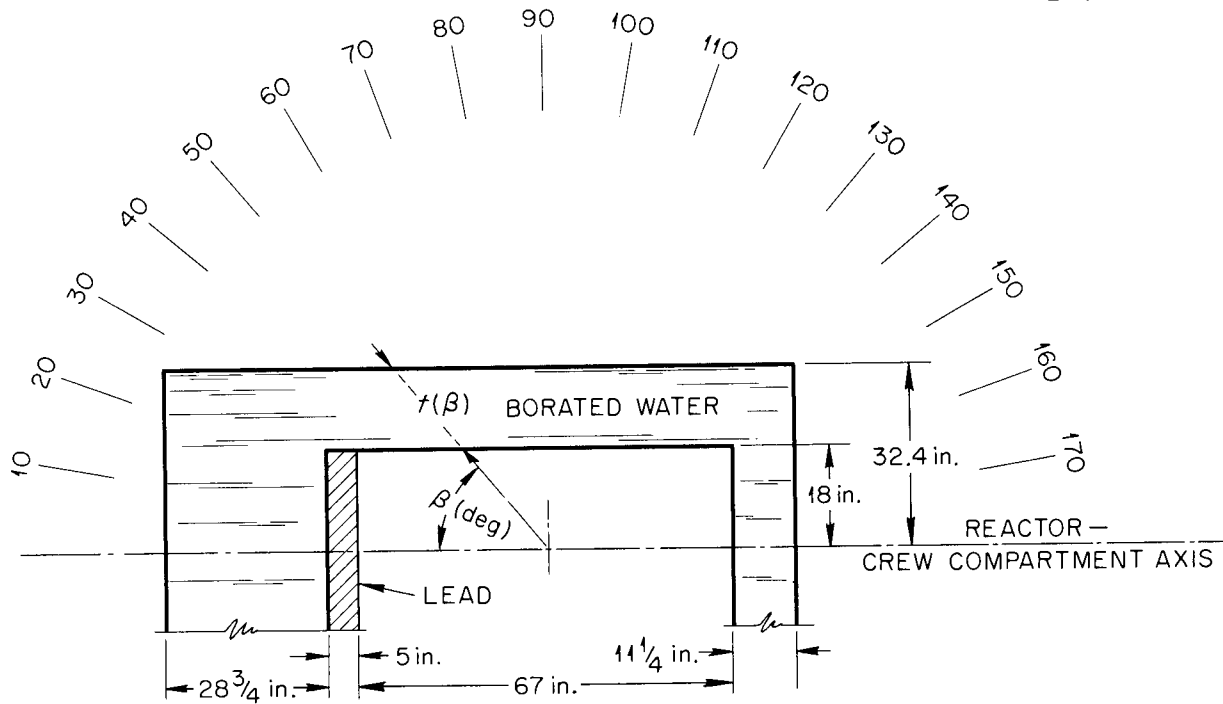


Fig. 6.2.17. Geometry for Case I Calculation of Air-Capture Gamma-Ray Dose Rate in the G-E Crew Compartment (Side Walls Shielded with Water Only).

$B'$  = dose buildup factor for the crew-compartment shielding material for gamma rays of the specified energy,

$$G(\beta, d, \theta', \rho) = \sum_E G'(\beta, E, d, \theta', \rho).$$

Calculations of the dose rate in the crew compartment resulting from air-capture gamma rays were carried out for the two crew-compartment configurations which were previously designated as cases I and III. (Figure 6.2.17 shows the geometry for case I, in which no lead side shielding is used.) The values of  $G'(\beta, E, d, \theta', \rho)$  and  $G(\beta, d, \theta', \rho)$  for case I with  $d = 64$  ft,  $\theta' = 0$  deg, and  $\rho = 45$  cm are given in Table 6.2.8. Corresponding plots of  $G'(\beta, E, d, \theta', \rho)$  as a function of  $\beta$  for various energies are given in Fig. 6.2.18. Figure 6.2.19 shows the composite curves of  $G(\beta, d, \theta', \rho)$  as a function of  $\beta$  for  $\theta' = 0$  deg and for  $\theta' = 180$  deg. The integrals under the curves give the predicted dose rates in the crew compartment for case I with the reactor on either the near side ( $\theta' = 0$  deg) or on the far side ( $\theta' = 180$  deg) of the reactor tank. The results are

$$D_{\theta'=0} = 7.22 \times 10^{-9} \text{ r/hr}\cdot\text{w}$$

and

$$D_{\theta'=180 \text{ deg}} = 1.71 \times 10^{-9} \text{ r/hr}\cdot\text{w} .$$

To obtain the dose rate for a different value of  $\rho$ , it is necessary merely to multiply the above

TABLE 6.2.8. VALUES OF THE FUNCTIONS  $G'(\beta; E, d, \theta', \rho)$  AND  $G(\beta, d, \theta', \rho)$  FOR CASE I

E (Mev)	$G'(\beta, E, d = 64 \text{ ft}, \theta' = 0 \text{ deg}, \rho = 45 \text{ cm}) (10^{-10} \text{ r/hr}\cdot\text{radian}\cdot\text{w})$														
	$\beta \text{ (deg)}$														
	30	40	50	60	70	80	90	100	110	120	130	140	150	160	170
10.816	4.46	6.05	7.10	7.79	8.09	8.02	7.67	7.12	6.38	5.40	4.30	3.11	3.32	2.65	1.42
9.156	0.33	0.46	0.55	0.60	0.63	0.62	0.60	0.55	0.50	0.42	0.33	0.24	0.26	0.21	0.11
8.278	0.64	0.89	1.06	1.16	1.21	1.20	1.16	1.07	0.96	0.80	0.64	0.46	0.50	0.40	0.21
7.356	1.66	2.33	2.80	3.11	3.23	3.23	3.10	2.86	2.55	2.16	1.70	1.19	1.34	1.08	0.57
7.164	0.53	0.76	0.91	1.02	1.05	1.06	1.01	0.94	0.83	0.70	0.55	0.39	0.43	0.35	0.19
6.318	2.19	3.16	3.84	4.28	4.46	4.46	4.29	3.96	3.52	2.96	2.33	1.62	1.85	1.49	0.81
5.554	3.13	4.58	5.64	6.28	6.58	6.62	6.40	5.89	5.22	4.36	3.42	2.36	2.73	2.23	1.20
5.287	4.54	6.71	8.26	9.27	9.74	9.74	9.33	8.65	7.68	6.41	5.00	3.44	4.02	3.26	1.77
4.285	1.24	1.91	2.39	2.71	2.87	2.89	2.79	2.56	2.26	1.88	1.45	0.98	1.19	0.98	0.53
4.000	1.42	2.23	2.80	3.19	3.39	3.40	3.29	3.02	2.67	2.21	1.69	1.14	1.40	1.17	0.63
3.000	0.25	0.37	0.51	0.59	0.63	0.64	0.61	0.56	0.50	0.40	0.31	0.19	0.26	0.22	0.12
Total = $G(\beta, d, \theta', \rho)$	20.39	29.45	35.86	40.00	41.88	41.88	40.24	37.18	33.07	27.70	21.72	15.12	17.30	14.04	7.56

values by the factor  $f(\rho)$  given in Fig. 6.2.12. The values of  $G'(\beta, E, d, \theta', \rho)$  and  $G(\beta, d, \theta', \rho)$  for case III with  $d = 64 \text{ ft}$ ,  $\theta' = 0 \text{ deg}$ , and  $\rho = 45 \text{ cm}$  are given in Table 6.2.9, and the corresponding plots of  $G(\beta, d, \theta', \rho)$  as a function of  $\beta$  for  $\theta' = 0 \text{ deg}$  and  $\theta' = 180 \text{ deg}$  are presented in Fig. 6.2.20. The discontinuities in the curves (also observed in Table 6.2.9) are caused by the step function decreases in lead shielding along the side walls. The integrated results for case III are

$$D_{\theta'=0} = 3.82 \times 10^{-9} \text{ r/hr}\cdot\text{w}$$

and

$$D_{\theta'=180 \text{ deg}} = 8.39 \times 10^{-10} \text{ r/hr}\cdot\text{w} .$$

The factors  $f(\rho)$  may again be used to scale the results to other values of  $\rho$ .

**Conclusions.** – Plots of the air-capture gamma-ray dose rate at the center of the crew compartment for cases I and III are presented in the following section, along with other calculated gamma-ray dose-rate components. It should be mentioned that these results are only as accurate as the value employed for the microscopic radiative capture cross section for nitrogen,  $\sigma_c^N$ , which is given to only one significant figure ( $0.1 \pm 0.05 \text{ barn}$ ). Should a better estimate of this quantity be made available in the future, the results could be corrected by multiplication by the ratio of the new to the old cross sections. It should also be mentioned that the method for attenuating the air-capture gamma rays through the crew shield was fairly crude. Several new codes that use the Monte Carlo calculational technique will be written in the near future. These

2-01-059-164

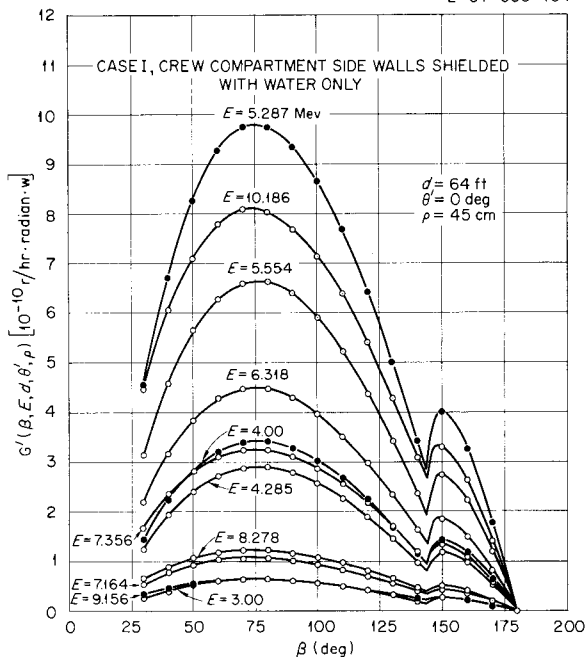


Fig. 6.2.18. Differential Air-Capture Gamma-Ray Dose Rates at the Center of the G-E Crew Compartment Resulting from Photons of Initial Energy  $E$  (Case I,  $\theta' = 0$  deg).

2-01-059-168

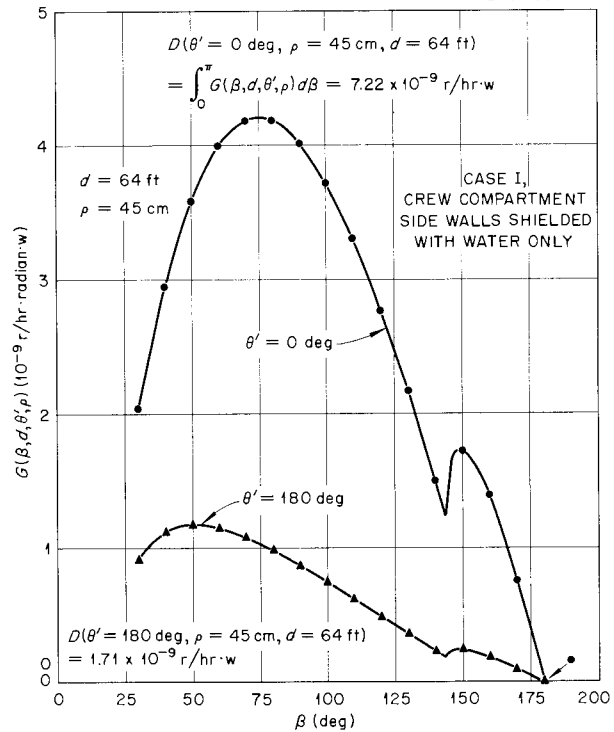


Fig. 6.2.19. Differential Air-Capture Gamma-Ray Dose Rates at the Center of the G-E Crew Compartment (Case I,  $\theta' = 0$  and  $180$  deg).

codes can be used to determine the dose rate inside a crew compartment if the angular and energy distributions are known for the gamma rays incident on the outside of the shield.

Comparison of the Total Calculated Dose Rate with the Measured Dose Rate

F. L. Keller

The predicted gamma-ray dose rate in air 64 ft from the center of the reactor tank is plotted in Fig. 6.2.21 as a function of  $\rho$  for  $\theta = 180$  deg. This curve represents the summary of the results from the calculations of the dose rates contributed by direct-beam, air-scattered, and air-capture gamma rays, which are plotted separately on the figure. It is obvious that the air-capture gamma rays do not contribute significantly to the total dose rate; therefore the total curve consists almost entirely of direct-beam and air-scattered gamma rays. When the predicted total dose rate is compared with the measured dose rate (also plotted on Fig. 6.2.21), it can be seen that for small values of  $\rho$  and  $\theta = 180$  deg (that is, for reactor positions close to the side of the reactor tank away from the point of observation) the agreement is quite poor. This is attributed to the inadequacy of the current methods of calculating dose rates resulting from air-scattered gamma rays when the emergent gamma rays leave the reactor shield in rearward directions with respect to the reactor-crew compartment axis. This should be expected, since multiple

TABLE 6.2.9. VALUES OF THE FUNCTIONS  $G'(\beta, E, d, \theta', \rho)$  AND  $G(\beta, d, \theta', \rho)$  FOR CASE III

E (Mev)	$G'(\beta, E, d = 64 \text{ ft}, \theta' = 0 \text{ deg}, \rho = 45 \text{ cm}) (10^{-10} \text{ r/hr}\cdot\text{radian}\cdot\text{w})$														
	$\beta$ (deg)														
	30	35.5	36	46	55.5	56	70	80	90	90	100	120	145	153.5	154
10.816	0.44	0.74	1.00	1.67	2.25	2.73	3.34	3.39	3.25	4.63	4.25	3.03	1.05	1.08	4.24
9.156	0.04	0.07	0.09	0.15	0.20	0.24	0.27	0.28	0.27	0.37	0.34	0.26	0.09	0.09	0.26
8.278	0.08	0.13	0.17	0.28	0.38	0.45	0.55	0.56	0.55	0.74	0.67	0.48	0.16	0.18	0.49
7.356	0.22	0.37	0.48	0.79	1.07	1.27	1.52	1.56	1.52	2.03	1.85	1.32	0.44	0.51	1.31
7.164	0.07	0.12	0.16	0.26	0.35	0.41	0.49	0.51	0.50	0.66	0.61	0.43	0.15	0.17	0.43
6.318	0.33	0.54	0.70	1.16	1.54	1.81	2.17	2.23	2.17	2.85	2.62	1.86	0.63	0.75	1.83
5.554	0.50	0.84	1.07	1.78	2.35	2.76	3.33	3.45	3.36	4.34	4.00	2.81	0.94	1.16	2.72
5.287	0.76	1.27	1.59	2.70	3.60	4.20	4.99	5.11	4.97	6.37	5.86	4.15	1.39	1.74	4.06
4.285	0.23	0.39	0.50	0.84	1.10	1.28	1.55	1.60	1.56	1.97	1.81	1.26	0.41	0.56	1.20
4.000	0.28	0.47	0.60	1.00	1.33	1.54	1.85	1.93	1.86	2.34	2.14	1.50	0.48	0.67	1.43
3.000	0.04	0.08	0.11	0.19	0.26	0.30	0.37	0.38	0.37	0.46	0.42	0.29	0.09	0.14	0.27
Total $= G(\beta, d, \theta', \rho)$	2.99	5.02	6.47	10.82	14.43	16.99	20.43	21.00	20.38	26.76	24.57	17.39	5.83	7.05	18.24

scattering becomes very important when the gamma rays leave in the rearward direction, whereas only single scattering is considered in the air-scattering probability curves which are in current use. When the gamma rays are emitted in the forward direction, the contribution of air-scattered gamma rays to the total dose rate is very small compared with the contribution of direct-beam gamma rays so that the accuracy of the air-scattering probability curves in this case cannot be ascertained. Work is currently under way in conjunction with WADC on a program designed to obtain more reliable gamma-ray air-scattering probabilities from a Monte Carlo calculation which includes all orders of scattering.

The final calculated results which were obtained for the gamma-ray dose rates in the crew compartment are compared with measured results in Figs. 6.2.22 through 6.2.25. These curves confirm the previous statements that the contribution from air-capture gamma rays should predominate when the reactor is near the tank wall on the side away from the crew compartment ( $\theta = 180$  deg) and that the direct-beam contribution should predominate when the reactor is on the side near the crew compartment ( $\theta = 0$  deg). It is again seen that the agreement is best when the reactor is on the side of the tank near the crew compartment. It may be noted, however, that the calculated dose-rate curve lies below the measured curve over the entire region. It should be pointed out that such a difference should be expected in any region where the contribution from direct-beam gamma rays which have been scattered in the side wall is appreciable

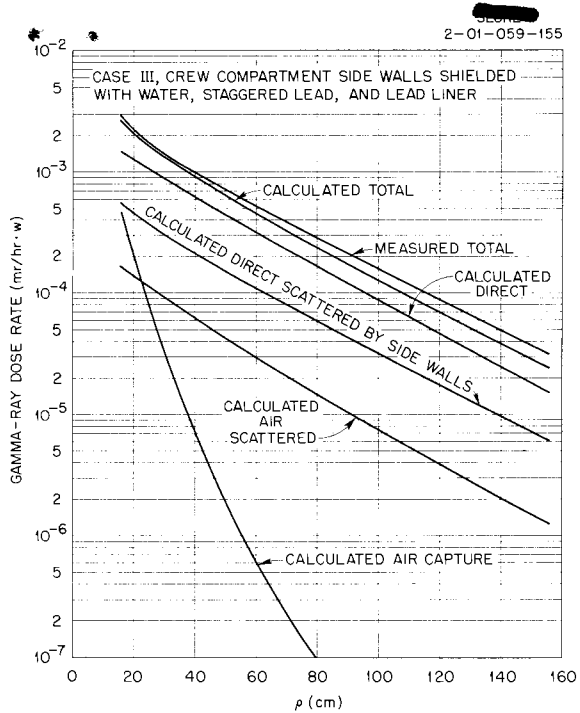


Fig. 6.2.24. Comparison of Measured and Calculated Gamma-Ray Dose Rates at the Center of the G-E Crew Compartment (Case III, TSF Reactor at  $\theta = 0$  deg).

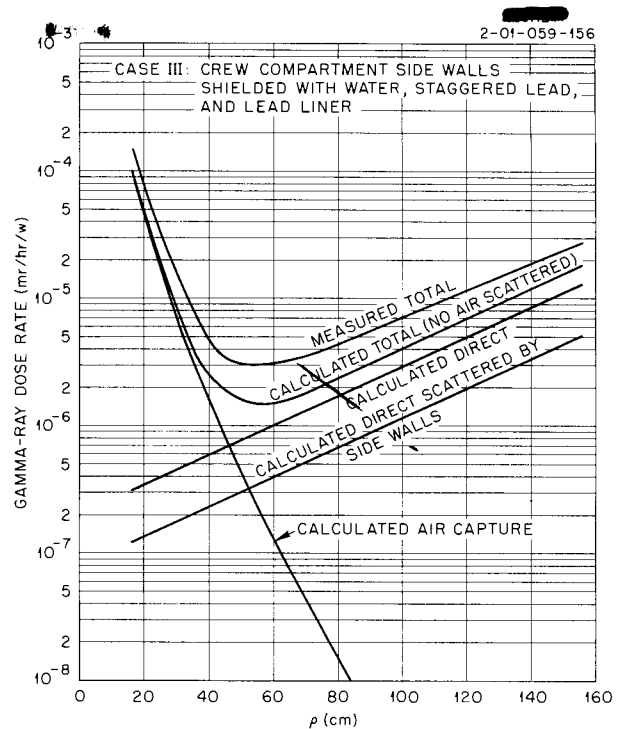


Fig. 6.2.25. Comparison of Measured and Calculated Gamma-Ray Dose Rates at the Center of the G-E Crew Compartment (Case III, TSF Reactor at  $\theta = 180$  deg).

program for calculating crew-compartment attenuations is being coded at ORNL, and a reliable calculation of the contribution from air-scattered gamma rays should be possible as soon as this and the Monte Carlo program at WADC, which was mentioned previously, are completed.

OPTIMIZATION OF A DIVIDED NEUTRON AND GAMMA-RAY SHIELD OVER A MISSION PROFILE

S. K. Penny  
C. A. Goetz<sup>17</sup>

A. T. Futterer<sup>17</sup>  
V. J. Sholund<sup>18</sup>

A divided neutron and gamma-ray shield configuration has been calculated for a specified total dose in the crew compartment rather than for the usual dose-rate restriction. The most recent optimization methods developed at ORNL were used along with the latest experimental data from the Tower Shielding Facility.

The reactor-crew compartment system that was selected was a Pratt & Whitney NJ-2A reactor, shielded with alkylbenzene-350 and lead, and a cylindrical crew compartment (86 cm in radius and 500 cm long) shielded with plastic and lead. Some additional shielding was available

<sup>17</sup>Pratt & Whitney Aircraft.

<sup>18</sup>Lockheed Aircraft Corp.

during certain legs of the mission from the chemical fuel tanks placed between the reactor and the crew compartment. The reactor-to-crew-compartment separation distance was assumed to be 47 ft.

The total mission dose was limited to 26.67 rem in the crew compartment with a 3/1 ratio of gamma-ray dose to neutron dose. The dose-rate criterion at 50 ft from the reactor was taken to be 50,000 rep/hr, this rate being chosen to limit the radiation damage of airplane components.

The mission profile included the variations in altitude, reactor power, and fuel-tank conditions shown in Table 6.2.10.

TABLE 6.2.10. MISSION PROFILE DATA

Condition	Time (hr)	Altitude (ft)	Power (Mw)
Take off and climb	0.3	0 to 28,000	320
Cruise out	19.17	28,000	320
Accelerate	0.23	28,000 to 52,500	320 to 206
Dash	0.87	52,500	206
Descend	0.065	52,500 to 42,000	206 to 200
Cruise back	20.4	42,000	200
Descend and land	0.3	42,000 to 0	200 to 320
Total	41.335		

#### Optimization of the Neutron Shield

The method used for the optimization of the neutron shield was the same as that outlined previously,<sup>19,20</sup> except that the alkylbenzene, chemical fuel, and plastic were replaced by water in the expressions for dose rate. The equivalent water thicknesses were determined by the ratio of hydrogen densities, but care was taken to ensure that the weight expressions would give the weight of the actual materials. The usual assumption was made that the neutron shield could be designed first, since replacing some neutron shielding with gamma-ray shielding should not appreciably affect the neutron dose rate.

The variation of the dose rate with reactor power, fuel tank conditions, and altitude was taken into account in a rather simple way: the dose rate resulting from direct-beam radiation was normalized to a 320-Mw power, empty fuel tanks, and a 1000-ft altitude. The variation with power was taken into account by a simple ratio. The variation with altitude was also taken into account by a simple ratio which was obtained from data taken at various altitudes, including the 1000-ft level, by the airborne shielding program at Convair.<sup>21</sup> The variation of the dose rate

<sup>19</sup>M. F. Valerino and F. L. Keller, *ANP Quar. Prog. Rep. Sept. 10, 1955*, ORNL-1947, p 205.

<sup>20</sup>S. K. Penny, *ANP Quar. Prog. Rep. March 10, 1956*, ORNL-2061, Part IV, p 54.

<sup>21</sup>C. F. Cook, *First Semiannual ANP Shielding Information Meeting, May 7-8, 1956, Volume 1*, ORNL-2115, Paper I-D (July 2, 1956).

with fuel tank conditions entered into the calculation only for the radiation from conical shells 1 and 2 of the reactor shield (see Fig. 6.2.26). These fuel tanks were considered to be full up to the dash and were thick enough to be black to radiation. During the dash the fuel was considered to be effectively black about 90% of the time. For the remainder of the mission, tanks 1 and 2 were considered to be empty. Therefore the mission profile was taken into account by multiplying the normalized dose rate by the altitude and power ratios and by 0, 1/10, or 1, depending on the fuel tank condition, and finally by the time interval of the particular leg. The fuel tank on the crew-compartment rear (No. 3) was a reserve tank and was never considered to be empty. The results of the neutron optimization are shown in Table 6.2.11.

2-01-059-178A

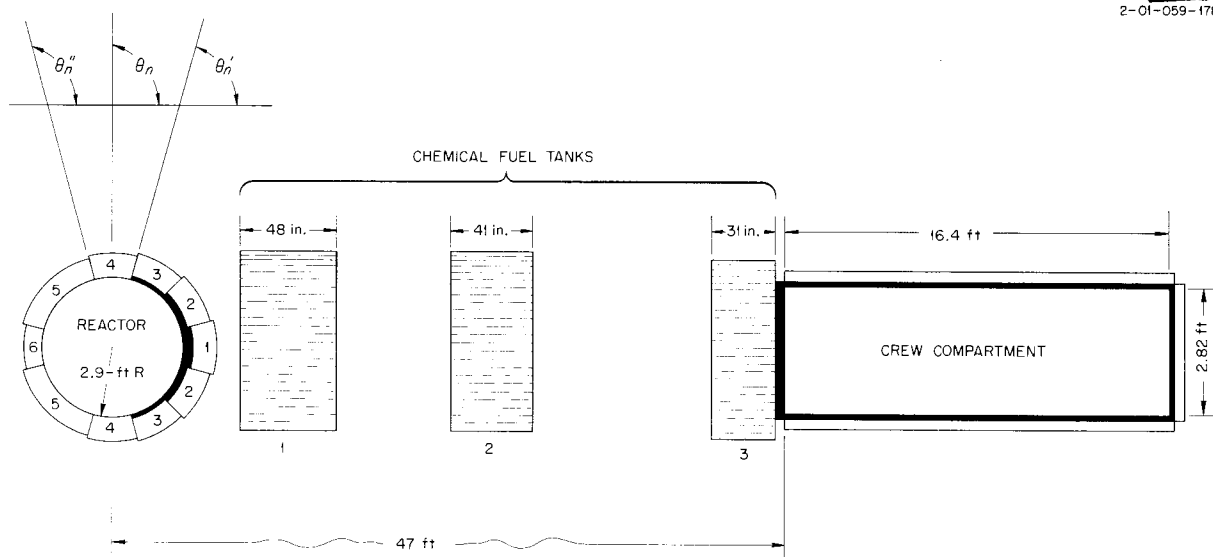


Fig. 6.2.26. Geometry for Optimization of a Divided Shield Over a Mission Profile.

### Optimization of the Gamma-Ray Shield

The procedure used for the optimization of the gamma-ray shield was somewhat similar to that for the neutron shield. The dose rates from both primary and secondary sources were calculated by methods reported previously,<sup>22</sup> and the variations of the dose rates with altitude, reactor power, and fuel tank conditions were handled the same way that they were for the neutron calculation. With the neutron shielding in place and no lead, the maximum total dose rate at 50 ft was 30,200 rep/hr, which well satisfied the dose-rate criterion. For the gamma-ray shield optimization the reactor shielding was again divided into conical shells of the same angular width as those used in the neutron shield optimization (see Fig. 6.2.26). The direct-beam radiation and the radiation scattered into the sides of the crew compartment were considered in

<sup>22</sup>J. B. Dee et al., ANP Quar. Prog. Rep. Dec. 10, 1955, ORNL-2012, Part IV, p 25.

TABLE 6.2.11. NEUTRON SHIELDING FOR REACTOR AND CREW COMPARTMENT

Shield Section	Thickness (cm)	Weight (tons)
Reactor shield* (alkylbenzene)		
0-15 deg	28.6	0.079
15-45 deg	30.6	0.60
45-75 deg	38	1.23
75-105 deg	34	1.19
105-165 deg	24.8	1.08
165-180 deg	22.6	0.048
Crew compartment (plastic)		
Side	14.65	4.77
Rear	0	0
Total		9.00

\*In conical shell sections with the polar axis being the reactor-crew compartment axis (see Fig. 6.2.26).

the calculation, the radiation scattered into the rear being neglected. The primary direct beam was assigned an angular distribution of  $\cos^{20} \theta$  at the surface of the shield, while the secondary direct-beam angular distribution was taken to be  $\cos \theta$ . The scattering calculation made use of the NDA air-scattering curves,<sup>23</sup> which were modified to include angular distributions at the reactor shield surface.<sup>24</sup> The energy of the gamma rays entering the crew compartment was assumed to be 3 Mev, which is conservative as far as the energy dependence goes. Since the method of calculation is exactly analogous to the method used for the neutron optimization, only the equations for the various steps in the iteration procedure will be given here.

The components of the dose in the crew compartment from radiation leaving the  $n$ th conical shell are

$$D_n^{p,d} = G_n D_{\text{NJ-2A}}^p(l, T_n, t_n) e^{-0.465t_r}$$

= direct-beam radiation from primary gamma rays,

$$D_n^{s,d} = H_n D_{\text{NJ-2A}}^s(l, T_n) e^{-0.465t_r}$$

= direct-beam radiation from secondary gamma rays,

$$D_n^{p,s} = M_n D_{\text{NJ-2A}}^p(l, T_n, t_n) e^{-t_s/\lambda(\theta_n, m)}$$

= scattered radiation from primary gamma rays,

$$D_n^{s,s} = N_n D_{\text{NJ-2A}}^s(l, T_n) e^{-t_s/\lambda(\theta_n, m')}$$

= scattered radiation from secondary gamma rays,

<sup>23</sup>E. P. Blizard and H. Goldstein (eds.), *Report of the 1953 Summer Shielding Session*, ORNL-1575, p 170 (June 14, 1954).

<sup>24</sup>D. R. Otis and H. C. Woodsum, *The Effect of Angular Distribution at the Shield Surface on the Gamma Ray Air Scattering Probabilities*, ORNL CF-56-5-73 (June 6, 1956).

ANP PROJECT PROGRESS REPORT

where

- $l$  = reactor-crew compartment separation distance,
- $T_n$  = thickness of alkylbenzene on the  $n$ th conical shell of the reactor,
- $t_n$  = thickness of lead on the  $n$ th conical shell,
- $t_r$  = thickness of lead on the rear of the crew compartment,
- $t_s$  = thickness of lead on the side of the crew compartment,
- $1/0.465$  = relaxation length in lead for 3-Mev gamma rays,
- $D_{\text{NJ-2A}}^p$  = direct-beam radiation from primary gamma-ray sources in the reactor and heat exchanger,
- $D_{\text{NJ-2A}}^s$  = direct-beam radiation from secondary gamma-ray sources at the lead-water interface,

$$G_n = \sum_i \eta_i \frac{\overline{P_i}}{P_0} \gamma_i (\cos^{m+1} \theta_n' - \cos^{m+1} \theta_n'') e^{-0.031T_{r'}} ,$$

$$H_n = \sum_i \eta_i \frac{\overline{P_i}}{P_0} X_i (\cos^{m'+1} \theta_n' - \cos^{m'+1} \theta_n'') e^{-0.031T_{r'}} ,$$

$$M_n = \sum_i \eta_i \frac{\overline{P_i \rho_i}}{P_0 \rho_0} u_i (4\pi l^2) (5.5 \times 10^5) \frac{1500}{l} \frac{f'(\theta_n)}{\sin \theta_n} \Big]_{m, T_s} (\cos \theta_n' - \cos \theta_n'') ,$$

$$N_n = \sum_i \eta_i \frac{\overline{P_i \rho_i}}{P_0 \rho_0} v_i (4\pi l^2) (5.5 \times 10^5) \frac{1500}{l} \frac{f'(\theta_n)}{\sin \theta_n} \Big]_{m', T_s} (\cos \theta_n' - \cos \theta_n'') ,$$

- $T_{r'}$  = thickness of reserve chemical fuel tank,
- $1/0.031$  = relaxation length of 3-Mev gamma rays in the chemical fuel,
- $T_s$  = thickness of plastic on crew-compartment sides,
- $\eta_i$  = time interval in the  $i$ th leg of the mission,

$$\frac{\overline{P_i}}{P_0} = \text{average ratio of reactor power in the } i\text{th leg to 320 Mw,}$$

$$\frac{\overline{\rho_i}}{\rho_0} = \text{average ratio of dose rate at the altitude in the } i\text{th leg to that at 1000 ft,}$$

$\gamma_i, X_i, u_i, v_i$  = factors to take into account the fuel tank conditions in the  $i$ th leg,

$$\frac{f'(\theta_n)}{\sin \theta_n} \Big]_{m, T_s} = \text{probability of a 3-Mev gamma ray from the } n\text{th conical shell scattering into the side of the crew compartment (evaluated for no lead, } T_s \text{ cm of plastic, and an angular distribution of } \cos^m \theta),$$

$\lambda(\theta_n, m)$  = relaxation length in lead on the side of the crew compartment for gamma rays leaving the  $n$ th conical shell with an angular distribution of  $\cos^m \theta$  [evaluated from  $f'(\theta_n)/\sin \theta_n$  as a function of lead thickness for  $T_s$  cm of plastic].

The total dose rate in the crew compartment is

$$D = \sum_n \left( D_n^{p,d} + D_n^{s,d} + D_n^{p,s} + D_n^{s,s} \right) .$$

The derivatives of the total dose with respect to lead thicknesses are

$$\frac{\partial D}{\partial t_s} = - \sum_n \left[ \frac{D_n^{p,s}}{\lambda(\theta_n, m)} + \frac{D_n^{s,s}}{\lambda(\theta_n, m')} \right] ,$$

$$\frac{\partial D}{\partial t_r} = -0.465 \sum_n \left( D_n^{p,d} + D_n^{s,d} \right) ,$$

$$\frac{\partial D}{\partial t_n} = -0.472 \left( D_n^{p,d} + D_n^{p,s} \right) \text{ (ref 25).}$$

The total weight of the lead may be written as

$$W = \frac{2\pi\rho_{Pb}}{3} \sum_n \left[ (t_n + a)^3 - a^3 \right] (\cos \theta_n' - \cos \theta_n'') + \\ + \pi\rho_{Pb} \left\{ R_c^2(t_s + t_n) + L_c \left[ (R_c + t_s)^2 - R_c^2 \right] \right\} ,$$

where

$\rho_{Pb}$  = density of lead,

$R_c$  = radius of crew compartment,

$L_c$  = length of crew compartment.

The Lagrangian multipliers for the sides and rear of the crew compartment and for the  $n$ th conical shell at the reactor are

$$L_s = - \frac{\partial D / \partial t_s}{\partial W / \partial t_s} ,$$

$$L_r = - \frac{\partial D / \partial t_r}{\partial W / \partial t_r} ,$$

$$L_n = - \frac{\partial D / \partial t_n}{\partial W / \partial t_n} , \quad (n = 1, 2, 3, \dots) .$$

<sup>25</sup> Experimentally the relaxation length of secondary gamma rays with respect to lead on the reactor is essentially infinite. The relaxation length of the primary direct gamma rays in lead is 1/0.472.

ANP PROJECT PROGRESS REPORT

In the optimized system

$$L = L_s = L_r = L_n .$$

By defining

$$\frac{1}{\overline{\lambda_s^p}} \equiv \frac{\sum_n D_n^{p,s} / \lambda(\theta_{n,m})}{\sum_n D_n^{p,s}}$$

and

$$\frac{1}{\overline{\lambda_s^s}} \equiv \frac{\sum_n D_n^{s,s} / \lambda(\theta_{n,m'})}{\sum_n D_n^{s,s}} ,$$

the estimate of  $L$  (equating  $L_s$  and  $L_r$ ) becomes

$$L = \frac{D + (\overline{\lambda_s^p} / \overline{\lambda_s^s} - 1) \sum_n D_n^{s,s}}{\overline{\lambda_s^p} \partial W / \partial t_s + 1/0.465 \partial W / \partial t_r} .$$

Further, if

$$e^{-t_s / \overline{\lambda_s^p}} \equiv \frac{\sum_n D_n^{p,s}}{\sum_n D_n^{p,s} e^{t_s / \lambda(\theta_{n,m})}} ,$$

$$e^{-t_s / \overline{\lambda_s^s}} \equiv \frac{\sum_n D_n^{s,s}}{\sum_n D_n^{s,s} e^{t_s / \lambda(\theta_{n,m'})}} ,$$

and

$$\alpha \equiv 0.465 \frac{\partial W / \partial t_s}{\partial W / \partial t_r} \overline{\lambda_s^p} ,$$

the approximate relation between  $t_s$  and  $t_r$  [denoted by  $t_r = U(t_s)$  and found by equating  $L_s$  and  $L_r$ ] is

$$\alpha e^{-0.465 t_r} \sum_n \left[ G_n D_{\text{NJ-2A}}^p(l, T_n, t_n) + H_n D_{\text{NJ-2A}}^s(l, T_n) \right]$$

$$= e^{-t_s / \overline{\lambda_s^p}} \sum_n M_n D_{\text{NJ-2A}}^p(l, T_n, t_n) + (\overline{\lambda_s^p} / \overline{\lambda_s^s}) e^{-t_s / \overline{\lambda_s^s}} \sum_n N_n D_{\text{NJ-2A}}^s(l, T_n) .$$

The approximate relations between  $t_n$  and  $t_s$  [denoted by  $t_n = V(t_s)$  and found by equating  $L_n$  to  $L$  and using  $t_n = U(t_s)$ ] are

$$\frac{\partial W / \partial t_n}{0.472 D_{\text{NJ-2A}}^p(l, T_n, t_n)} = \frac{1}{L} \left[ G_n e^{-0.465 U(t_s)} + M_n e^{-t_s / \lambda(\theta_{n,m})} \right] .$$

The right side of the equation above is a function of the conical shell and  $t_s$ ; the left side is a function of the conical shell and  $t_n$ .

The approximate relation between  $t_s$  and  $L_s$  [denoted by  $L_s = Z(t_s)$  or  $t_s = Z^{-1}(L_s)$  and found by using  $t_n = V_n(t_s)$ ] is

$$L_s = \frac{1}{\partial W / \partial t_s} \sum_n \left\{ \frac{M_n D_{\text{NJ-2A}}^p [l, T_n, V_n(t_s)] e^{-t_s / \lambda(\theta_n, m)}}{\lambda(\theta_n, m)} + \frac{N_n D_{\text{NJ-2A}}^s (l, T_n) e^{-t_s / \lambda(\theta_n, m')}}{\lambda(\theta_n, m')} \right\} .$$

By going through the preceding steps and equating  $L$  to  $L_s$  in the last step,

$$t_s = Z^{-1}(L) ,$$

$$t_n = V_n[Z^{-1}(L)] ,$$

and

$$t_r = U[Z^{-1}(L)] .$$

These thicknesses are then used in the next iteration. The results of the optimization are given in Table 6.2.12. The neutron optimization procedure is probably more realistic than the gamma-ray optimization procedure, since it is based more on experimental data.

TABLE 6.2.12. GAMMA-RAY SHIELDING FOR REACTOR AND CREW COMPARTMENT

Shield Section	Lead Thickness (cm)	Weight (tons)
Reactor shield*		
0-15 deg	12.6	0.30
15-45 deg	8.2	1.42
45-75 deg	1.3	0.36
75-105 deg	0	0
105-165 deg	0	0
165-180 deg	0	0
Crew compartment		
Side	0.48	1.76
Rear	9.0	2.61
Total		6.45

\*In conical shell sections with the polar axis being the reactor-crew compartment axis (see Fig. 6.2.26).